Shadow Information Spaces: Combinatorial Filters for Tracking Targets

Jingjin Yu, *Student Member, IEEE*, and Steven M. LaValle, *Member, IEEE*

***Abstract*—This paper introduces and solves a problem of maintaining the distribution of hidden targets that move outside the field of view while a sensor sweep is being performed, resulting in a generalization of the sensing aspect of visibility-based pursuit-evasion games. Our solution first applies information space concepts to significantly reduce the general complexity so that information is processed only when the shadow region (all points invisible to the sensors) changes combinatorially or targets pass in and out of the field of view. The cases of distinguishable, partially distinguishable, and completely indistinguishable targets are handled. Depending on whether the targets move nondeterministically or probabilistically, more specific classes of problems are formulated. For each case, efficient filtering algorithms are introduced, implemented, and demonstrated that provide critical information for tasks such as counting, herding, pursuit evasion, and situational awareness.**

***Index Terms*—Combinatorial filters, integer linear programming, shadow information spaces, target tracking, visibility based pursuit evasion.**

I. Introduction

IMAGINE a game of *hide-and-seek* is being played. After the hiders conceal themselves (subsequent relocations are allowed), the seekers, familiar with the environment, start to search for the hiders. Most people who played the game as school children know that an effective search begins with the seekers checking places having high probabilities of containing a hider, from previous experience: a closet, an attic, a thick bush, and so on. After the most likely locations are exhausted, the next step is to carry out a systematic search of the environment, possibly with some seekers guarding certain escape routes. Occasionally, during the game, hiders may attempt to relocate themselves to avoid being found. While the hiders succeed sometimes, they may end up being spotted by the seekers and are instead getting found earlier.

Manuscript received January 5, 2011; revised June 24, 2011; accepted October 24, 2011. Date of publication December 23, 2011; date of current version April 9, 2012. This paper was recommended for publication by Associate Editor V. Isler and Editor G. Oriolo upon evaluation of the reviewers' comments. This work was supported in part by National Science Foundation under Grant 0904501 (IIS Robotics) and Grant 1035345 (Cyberphysical Systems), Defense Advanced Research Projects Agency's Sensors, Topology, and Minimalist Planning under Grant HR0011-05-1-0008, and Multidisciplinary University Research Initiative/Office of Naval Research under Grant N00014-09-1-1052.

J. Yu is with the Department of Electrical and Computer Engineering, University of Illinois at Urbana-Champaign, Urbana, IL 61801 USA (e-mail: jyu18@uiuc.edu).

S. M. LaValle is with the Department of Computer Science, University of Illinois at Urbana-Champaign, Urbana, IL 61801 USA (e-mail: lavalle@uiuc.edu).

Color versions of one or more of the figures in this paper are available online at http://ieeexplore.ieee.org.

Digital Object Identifier 10.1109/TRO.2011.2174494

Although it is child's play, this game captures the two key interacting ingredients of pursuit evasion (PE) games: passively estimating the distribution of hidden targets and actively planing to reduce the uncertainty of this distribution. The general goal in PE research is to algorithmically clear evading targets from a workspace. As pursuers try to ensure that the workspace is evader free, they always need to maintain the pursuit status, remembering whether a region outside of the pursuers' field-of-view (FOV) is contaminated or cleared (one bit of information per region).

This paper, expanding upon [51] and [52], studies exactly this passive ingredient of PE games, i.e., reasoning about the information residing in unobservable regions of the environment. In particular, we introduce the notion of *filters* over *shadow information spaces* for tracking moving targets in unobservable regions, as a generalization of this aspect of PE. To achieve this, we first process sensor observation history and compress it in a lossless fashion for our task classes, for storage and effective computation. Next, depending on whether the targets of interest are moving nondeterministically or probabilistically, concrete problems are formulated and solved by carefully manipulating and fusing observation and data. At a higher level, at any time, our algorithm can estimate the number of targets hidden in regions that are not directly observable. We note that, although the active problem of planning a pursuit path is not addressed in this paper, heuristic search strategies can be readily implemented on the space of filter outputs.

The mathematical study of PE games dates back to at least four decades ago, with its roots in differential games [15]–[17]. Although optimal strategies for differential PE games are still actively pursued [2], [25], [29], [46], a variant of differential PE games, i.e., visibility-based PE, has received much attention recently. Development of visibility-based PE games can be traced back to [32], in which a PE game on discrete graphs is introduced with the goal of sweeping evaders residing on continuous edges of a graph. The evaders can move arbitrarily fast, but must move continuously. The Watchman Route problem [8], [9], which was formulated 12 years later as a variant of the Art Gallery problems [27], [38], involves finding shortest route to clear static intruders. An intruder is considered cleared if a line of sight exists between the intruder and a point of the watchman route.

Influenced by these two threads of research, Suzuki and Yamashita [42] defined what we know today as visibility-based PE games in which the discrete graph domain is replaced by a path-connected interior of a 2-D polygon, and a continuously moving evader is considered to be cleared if it falls into the visible region of a pursuer (in this case, the pursuer is equipped with

two flashlights and is called a 2-searcher). Thinking along the same lines as the Art Gallery problems, it was soon established that for a pursuer with an omnidirectional infinite range sensor (i.e., an ∞-searcher), it is NP-hard to decide the minimum number of pursuers needed for the class of simply connected polygons [14], [24]. The insight that bitangents and inflections fully capture the critical changes leads to a generalization from polygons to curved environments [23] and form the basis of some critical events that are used in our work.

Various sensing and motion capabilities are explored in visibility-based PE. Interestingly, it turns out that a 2-searcher is as capable as an ∞-searcher in simple polygons [31]. Pursuers with a single flashlight/beam (a 1-searcher) are investigated in detail in [39] and [20], with the latter limiting the pursuer's motion to the boundary of the environment. Variations along this line include limited FOV [11], unknown environments [35], and bounded speed [44]. Another theme in PE games is to discretize time and put speed bounds on both pursuers and evaders. In this setting, sufficient conditions and strategies for a single pursuer to capture an evader are given to the classical lion-and-man problem in the first quadrant of the open plane [37]. This problem is then extended to $\mathbb{R}^n$ and multiple pursuers in [21] and multiple pursuers with limited range in [5]. Finally, PE is also studied in the probabilistic context [18], [47] and abstract metric spaces [1].

Since we provide algorithms for tracking moving targets, our work is also closely related to target tracking and enumeration. The problem of accurately counting the number of targets with overlapping footprints is solved with a novel approach of integrating over Euler characteristics in [3]. With a virtual sensor that reports visible features of polygonal environment, as well as indistinguishable targets, static targets are counted under various setups in [12]. A filtering algorithm is provided in [40] to count moving targets with a network of binary proximity sensors. In [48], simultaneous localization and mapping and detection and tracking of moving objects are combined to attack both problems at the same time. A specialization of our problem is investigated in [43] in which the sensor FOV becomes 1-D beams. Real-time people counting with a network of image sensors is studied in [50].

Another research area of relevance to this paper, especially the probabilistic formulations that we give in Section VI, is the study of *optimal search* [41], which proposes a Bayesian approach to maintain a target distribution and use that information to guide the planning of optimal search paths. The essential idea from optimal search is to plan a path to eliminate regions with highest probability of containing the targets. In doing so, optimal search algorithms allow the prediction of the *no-detection likelihood* [4], [7], [26], [49], which is the probability that the targets remain undiscovered at given stages of a search effort, even before the actual search is carried out. Although our work also seeks to maintain a target distribution along a given path, we focus on the computational problem of how *topological* changes of nonobservable components, which are *combinatorial* in nature, can be correctly and efficiently processed as the target distribution evolves. This topological/combinatorial element of target tracking exists whether the problem formulation is probabilistic or not. In this aspect, the problems that we address here are mostly orthogonal to classical optimal search problems, which cover environments (support surfaces of the distribution) that are mainly 2-D obstacle-less planes such as these appearing in typical maritime applications. As such, the results that are presented in this paper should benefit the extension of optimal search results to covering more diverse workspaces, such as urban areas and hilly terrains, where topological changes of nonobservable components are frequent.

The main contributions of this study are twofold. First, as explained earlier, we generalize visibility-based PE by introducing a richer class of problems and providing a framework as a submodule to systematically attack these problems. Second, the capability of effectively tracking hidden, moving targets, which is a general type of *situation awareness*, applies to a large class of time critical tasks in both civilian and national security applications. For example, in a fire evacuation scenario, knowing the possible/expected number of people trapped in various parts of a building, firefighters can better decide which part of the building should be given priority when they coordinate the search-and-rescue effort.

The rest of this paper is organized as follows. Section II provides a mathematical definition of what we mean by "shadows" and "component events," which can be best captured using a chronological sequence. Section III suggests the general problem of tracking hidden targets after bringing in moving targets and FOV events. Section IV formulates the problem of estimating the number of targets hidden in shadows for nondeterministically moving targets and establishes its polynomial time solvability using results from integer linear programming (ILP) theory. Section V shows how information spaces [22] can guide the design of efficient algorithms to solve the nondeterministic formulation in a more intuitive fashion. Section VI extends the problem formulation and solutions to probabilistically moving targets and imperfect sensors. We provide implementation, simulation results, and algorithmic analysis in Section VII and conclude this paper in Section VIII.

II. Component Events, Shadows, and Shadow Sequences

Intuitively, in the hide-and-seek game, the part of the world that is not observable is comprised of many components, each of which has a life span. To study the information flow in them, a formal definition of components is first in order; the temporal relationship among them then comes up naturally.

A. Component Events and Shadows

Let a nonempty set of robots move along continuous trajectories in a *workspace*, i.e., $W = \mathbb{R}^2$ or $W = \mathbb{R}^3$. Let the configuration space of the robots be $\mathcal{C}$. At some time t, there may be configuration space obstacles $\mathcal{C}_{\rm obs}$ which may vary over time, leaving $\mathcal{C}_{\rm free} := \mathcal{C} \backslash \mathcal{C}_{\rm obs}$ as the free configuration space. Let $q \in \mathcal{C}_{\rm free}$ be the configuration of the robots at time t. Returning to the workspace, there is a closed *obstacle region* $O(t) \subset W$, leaving $F(t) := W \backslash O(t)$ as the free space. The robots are equipped with sensors that allow them to make shared observations in a

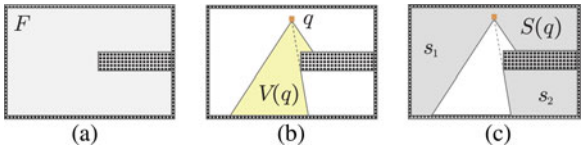

Fig. 1. (a) Environment and the free space, F. Note that in this example, the obstacle region is fixed; therefore, F is constant. (b) Visible region: $V(q)$. (c) Shadow region: $S(q)$, with two path components s_1, s_2.

joint *FOV* or *visible region* $V(q,t) \subset F(t)$. For convenience, we take the closure of $V(q,t)$ and assume that the visible region is always closed. Let $S(q,t) := F(t) \backslash V(q,t)$ be the *shadow region*, which may contain zero or more nonempty path connected components (path components for short). A path component is assumed to be nonempty unless otherwise specified. At any instant, $O(t), V(q,t)$, and $S(q,t)$ have disjoint interiors by definition, and $W = O(t) \cup V(q,t) \cup S(q,t)$. Fig. 1 shows $V(q), S(q)$ for a point robot holding a flashlight with $F \subset W = \mathbb{R}^2$, $\mathcal{C}_{\text{free}} \subset SE(2)$, which is the set of 2-D translations and rotations (here, we omit the parameter t from F, V, and S, since the obstacle region does not vary over time).

To observe how path components of the shadow region evolve over time, let the robots follow some path $\tau : [t_0, t_f] \to \mathcal{C}$, where $[t_0, t_f] \subset T \subset \mathbb{R}$ is a time interval. Let $Z = W \times T$. We may let $O : T \to Pow(Z)$ be the map that yields the obstacle region and define V, S as: $V, S : \mathcal{C} \times T \to Pow(Z)$. Since a path τ, parameterized over $t \in T$, is always assumed in the paper, we abusively write $V(t), S(t)$ in place of $V(\tau(t), t), S(\tau(t), t)$, respectively. In particular, we are interested in $S(t)$ and call it a *slice*. For any $(t_a, t_b) \subset [t_0, t_f]$, let the union of all slices over the interval

$$S(t_a, t_b) := \bigcup_{t \in (t_a, t_b)} S(t)$$

be called a *slab*, which is an open subset of Z. For any subset z of Z, define its projection onto the time axis as

$$\pi_t : Pow(Z) \to Pow(T)$$
$$z \mapsto \{t \mid (p,t) \in z \text{ for some } p \in W\}.$$

Let $s_{t,i} \subset S(t)$ denote the ith path component of $S(t)$ (assuming some arbitrary ordering). Let $s_{i'}$ denote the i'th path component of a slab $S(t_a, t_b)$ (again, assuming some arbitrary ordering). $S(t_a, t_b)$ is *homogeneous* if for all $t \in (t_a, t_b)$ and all i, there exists i' such that $s_{t,i} = S(t) \cap s_{i'}$ and, separately, $\pi_t(s_{i'}) = (t_a, t_b)$ for all i'.

A homogeneous slab is called *maximal* if it is not a proper subset of another homogeneous slab. The definition, then, partitions $S(t_0, t_f)$ into some m disjoint maximally homogeneous slabs plus some slices

$$S(t_0, t_f) = S(t_0, t_1) \cup S(t_1) \cup \cdots \cup S(t_{m-1}) \cup S(t_{m-1}, t_f).$$

That is, homogeneity of $S(t_0, t_f)$ is broken at $t_1, \ldots, t_{m-1}$. What exactly happens at $t_1, \ldots, t_{m-1}$? Let there be two homogeneous slabs $S(t_a, t_b)$ and $S(t_b, t_c)$ such that for some $k \in \{1, \ldots, m-1\}$, $t_{k-1} \le t_a < t_b = t_k < t_c \le t_{k+1}$. Letting s_i be an arbitrary path component of $S(t_a, t_b)$, at $t = t_b$, s_i may ($\overline{s}$ denotes the closure of s)

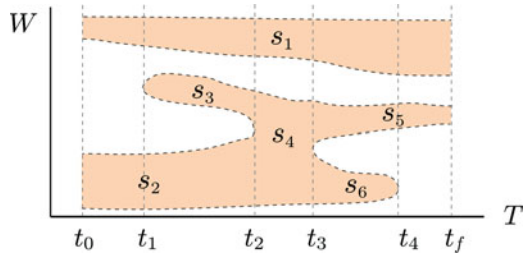

Fig. 2. Evolution of shadow regions: t_1: s_3 appears, t_2: s_2, s_3 merge into s_4, t_3: s_4 splits into s_5, s_6, t_4: s_6 disappears. The "sizes" of the shadow regions have no effect on the critical events.

1) *live on*, if there exists a path component $s_j \subset S(t_b, t_c)$ such that $\overline{s_i} \cap S(t_b) = \overline{s_j} \cap S(t_b) \neq \emptyset$;
2) *disappear*, if $\overline{s_i} \cap S(t_b) = \emptyset$.

Similarly, a path component $s_j \subset S(t_b, t_c)$ may

3) *appear*, if $\overline{s_j} \cap S(t_b) = \emptyset$.

Finally, a nonempty set of path components $\{s_i\}$ of $S(t_a, t_b)$ may

1) *evolve*, if there is a nonempty set of path components $\{s_j\}$ of $S(t_b, t_c)$ such that $|\{s_i\}| + |\{s_j\}| \ge 3$ and $\bigcup_i \overline{s_i} \cap S(t_b) = \bigcup_j \overline{s_j} \cap S(t_b) \neq \emptyset$ is a single path component of $S(t_b)$.

By definition, appear, disappear, and evolve are critical changes that only (and at least one of which must) happen between two adjacent maximally homogeneous slabs. We call these changes *component events*. With component events, homogeneity and maximality readily extend to path components of slabs. A path component $s_i \subset S(t_a, t_b)$ is called *homogeneous* if no component events happen to a subset of s_i in (t_a, t_b); s_i is called *maximal* if it is not a proper subset of another homogeneous path component.

At this point, a type of general position is assumed to avoid two tedious cases: 1) Four or more path components cannot be involved in an evolve event; and 2) two or more component events cannot occur at the same time. In practice, nongeneral position scenarios form a measure zero set and can be dealt with via small perturbations to the input if required. With such an assumption, exactly one component event happens between two maximally homogeneous slabs. Moreover, the evolve event can be divided into two sub events: *split* if $|\{s_i\}| = 1, |\{s_j\}| = 2$ and *merge* if $|\{s_i\}| = 2, |\{s_j\}| = 1$.

We now piece together the aforementioned definitions using an example illustrated in Fig. 2. Restricting to the time interval (t_0, t_f), there are five maximally homogeneous slabs, i.e., $S(t_0, t_1), \ldots, S(t_4, t_f)$. Certain proper subsets of one of these, such as $S(t_2^+, t_3^-)$ with $t_2 < t_2^+ < t_3^- < t_3$, are again homogeneous but no longer maximal; on the other hand, supersets, such as $S(t_2^-, t_3^+)$ with $t_2^- < t_2 < t_3 < t_3^+$, are no longer homogeneous. The slab $S(t_0, t_f) \subset Z$ has two path components (s_1 and $\text{Int}(\overline{s_2} \cup \overline{s_3} \cup \overline{s_4} \cup \overline{s_5} \cup \overline{s_6})$, where Int denotes the interior of a set) and six maximally homogeneous path components $s_1, \ldots, s_6$. The intersection of a vertical line at $t \in (t_0, t_f)$ with $S(t_0, t_f)$ corresponds to the slice $S(t)$. For convenience, it is assumed that $t = t_0$ is not a critical time in the sense that for each path component $s_{t_0,i} \subset S(t_0)$, $s_{t_0,i} = \overline{s_{i'}} \cap S(t_0)$ for some

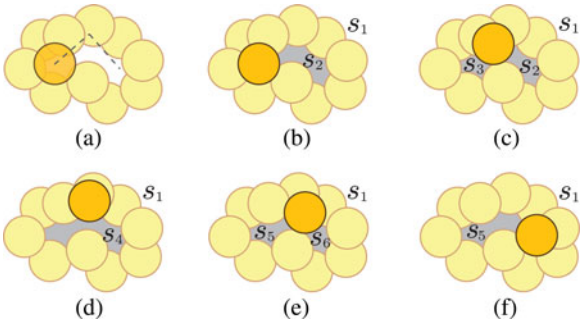

Fig. 3. Example of shadows and their indexing/labeling. (a) Set of spotlights and the path to be followed by the darker (orange) colored spotlight. (b) Initially, only shadow s_2 and unbounded shadow s_1 exist. (c) New shadow s_3 *appears*. (d) s_2, s_3 *merge* into a single shadow s_4. (e) s_4 *splits* into new shadows s_5, s_6. (f) s_6 *disappears*.

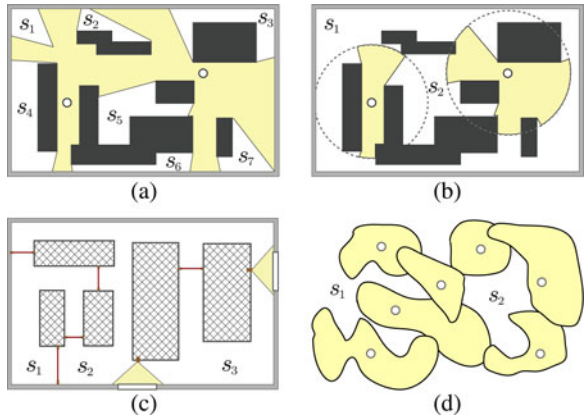

Fig. 4. (a) Two robots (white disks) carrying omnidirectional, infinite range sensors. The free space is partitioned into seven shadows. (b) When sensing range is limited, the topology of shadows changes; only two shadows are left. (c) Indoor environment guarded by fixed beam sensors (red line segments) and cameras (yellow cones). There are three connected shadows. (d) Simple mobile sensor network in which the white disks are mobile sensing nodes, with shaded regions being their sensing range at the moment. There are two shadows with s_1 being unbounded.

path component $s_{i'} \subset S(t_0, t_1)$. A similar assumption is made for $t = t_f$. Under this setup, there are four component events: 1) s_3 appears at $t = t_1$; 2) s_2 and s_3 merge to form s_4 at $t = t_2$; 3) s_4 splits into s_5, s_6 at $t = t_3$; and 4) s_6 disappears at $t = t_4$. In contrast, the path component $s_1 \cap S(t_0, t_1)$ lives on through $t_1, \ldots, t_4$.

Finally, in this section, we define the main concept of the paper: *shadow*. It is easy to see that maximally homogeneous path components are pairwise disjoint. Let such a path component be called a *shadow*; let $\{s_i\}$ be the set of shadows of $S(t_0, t_f)$; note that $S(t_0, t_f)$ is contained in the closure of $\cup_i s_i$. In the previous example, $\{s_i\} = \{s_1, \ldots, s_6\}$. For some $t \in (t_0, t_f)$, let a path component of $S(t)$ be labeled as $s_{t,i}$ if it is a slice of a shadow s_i. More precisely, $s_{t,i} = s_i \cap \{(p, t) \mid p \in W\}$. For $t = t_0$, $s_{t_0,i}$ is labeled such that $s_{t_0,i} = \overline{s_i} \cap S(t_0)$ for some path component $s_i \subset S(t_0, t_1)$. The same applies to the labeling of $s_{t_f,i}$. A path component of $S(t)$ has no label exactly when it is the border of two or more shadows of a slab. Since such labeling is unique, we drop time subscript of $s_{t,i}$ if t is fixed. In the rest of this paper, we use the set $\{s_i\}$ to denote both shadows and slices of shadows; we simply call both types of path components *shadows* when no confusion arises from the context. When we need to distinguish, the former will be called *workspace-time shadows* and the latter *workspace shadows*.

B. Shadows are Everywhere

To promote the intuition behind the mathematical definitions, let us look at a realistic example shown in Fig. 3(a). With the intention of guarding a planar region, spotlights are cast on the ground, creating a set of illuminated disks as shown. Assume that only the darker (orange) colored disk of light moves and follows the dashed line. For any position of the moving spotlight, the combined illuminated set can be thought of as the FOV. Its complement in the plane is the shadow region, in which targets cannot be directly observed. Initially, there are two connected components, which are labeled s_1 (unbounded) and s_2, in the shadow region. As the spotlight moves along the dashed line, we observe that shadows may appear, disappear, merge, and split, as illustrated in Fig. 3(b)–(f). We constructed this example so that the events and evolution of shadows match exactly these of the example from Fig. 2.

The naive example suggests that shadows and component events arise from very simple setups. Indeed, shadows and component events are ubiquitous, showing up whenever moving sensors are placed inside environments. We provide three additional examples to corroborate this point; many others could be presented. In Fig. 4(a), omnidirectional, infinite range sensors partition the 2-D environment into polygonal shadows. The component events happen exactly when the sensors make *inflection* and *bitangent* crossings (see aspect graphs [33]), which gives rises to the concept of *gaps* and *gap navigation trees* as discussed in [45]. If the sensors have limited viewing angle [11] or limited range [see Fig. 4(b)], alternate models governing visible and shadow regions are obtained. In Fig. 4(c), fixed infrared beams and surveillance cameras are placed inside a building, creating a set of three fixed shadows $s_1, s_2,$ and s_3. Such a setting is common in offices, museums, and shopping malls. As a last example, Fig. 4(d) shows a simplified mobile sensor network with coverage holes. In this case, the joint sensing range of the sensor nodes is the FOV and the coverage holes are the shadows, which fluctuate continuously even if the sensor nodes remain stationary (consider cellphone signals).

For some environments, shadows are readily available or can be effectively computed with high accuracy, such as visibility sensors placed in 2-D polygonal environments. In some other cases, shadows are not always easy to extract. As one example, estimating coverage holes in a wireless sensor network is rather hard, since it is virtually impossible to know whether a point p is covered unless a probe is dispatched to p to check. It is also well known that 3-D visibility structure is difficult to compute [28], [34]. Even though we do not claim to overcome such inherent difficulties in acquiring visibility region and/or shadows, the method presented here applies as long as a reasonably accurate characterization of the shadows is available.

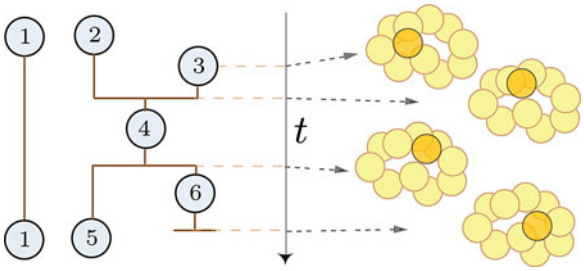

Fig. 5. Shadow sequence for the example from Fig. 3. The numbers in the circles represent the labels of the shadows. The four events marked on the time line, from top to bottom, are appear, merge, split, and disappear. As one would expect, this figure closely resembles Fig. 2.

C. Shadow Sequences

We conclude this section with the introduction of a *shadow sequence*, of which the importance will become more apparent in coming sections. When the shadows of $S(t_0, t_f)$ for a fixed path τ are put together, a sequential structure comes up. This structure, which we call a shadow sequence, captures the combinatorial changes of the labeled shadows through component events. A graphical illustration of the shadow sequence for the example in Fig. 3 is given in Fig. 5.

III. Targets, Field-of-View Events, and Imperfect Sensors

A. Targets

Our interest in shadows lies with maintaining information that is not directly observable by sensors. To effectively investigate how to track such information, we briefly characterize what we mean by information. We assume that there is a nonnegative integer number of *targets* in F, which are point entities that move arbitrarily fast but follow some continuous, unpredictable trajectories. The robots' sensors can detect certain *attributes* of these targets. We are interested in two types of attributes: location and identity.

Location: When the targets move in/out the sensors' FOV, their appearance/disappearance may be detected. Depending on the sensors' capabilities, at least two levels of precision are possible: 1) The sensors can tell whether the FOV contains no target or at least one. In other words, each sensor's output is *binary* (motion detector is a sensor of this type). 2) Each target inside the FOV can be precisely located and counted.

Identity: When multiple targets are present, it may be possible to tell them apart. That is, the sensors may be able to *distinguish* the targets in the FOV. Roughly speaking, the targets may be

1) *Fully distinguishable*. When targets possess unique IDs recognizable by the sensors, they are fully distinguishable.
2) *Indistinguishable*. Although it appears that full distinguishability is the most powerful, it is not always available due to sensor cost constraint or even desirable due to concerns such as privacy. It is not hard to make targets indistinguishable: In the sensor output, erase any attributes that can be used to distinguish among the targets.
3) *Partially distinguishable*. Everything between the previous two notions of distinguishability belongs to this class. For instance, targets may form *teams* that are distinguishable by color.

Location and identity are related—full distinguishability implies that the sensors should be able to locate targets in the FOV. On the other hand, tracking locations over time can be used to distinguish targets. However, these two attributes are not identical and it benefits to treat them orthogonally. For example, when colored teams of targets are present, a low-resolution overhead camera can easily tell whether a team is present in the FOV via a color scan, acting as a combination of binary location sensor and identity sensor. Given sensors that can detect some subsets of the aforementioned attributes of targets, each labeled shadow can be assigned one or more variables that describe these attributes of the targets residing in the shadow. Note that although we deal mostly with binary and integer variables in this paper, variables of other forms, such as real numbers, can also be incorporated over the structure of shadows and component events introduced here. When we consider targets in the shadows, a type of invariance arises.

Observation 1 In an environment with only component events, the number of targets hidden in a workspace-time shadow is invariant along its span over time; furthermore, a workspace-time shadow is a maximal set in which such invariance holds.

By the assumption that a hidden target moves continuously, its trajectory is contained in the same workspace-time shadow when no component events happen. Two workspace shadows, as different time slices of the same workspace-time shadow, must intersect the same number of such trajectories, since no target enters or exits the component in the time being. This yields the invariance. The second claim follows the definition of workspace-time shadow as a maximal union of all such workspace shadows.

B. Field-of-View Events

If a location sensor also has *memory*, it will be able to detect changes to the number of targets in the FOV during a short time interval. We call such a change a *field-of-view event* (FOV event for short), a second type of critical events. Furthermore, if the sensors know where FOV events happen, such events can be associated with corresponding shadows. For a shadow s_i, three FOV events are possible: 1) A target *enters* s_i from the FOV. 2) A target *exits* s_i into the FOV. 3) Nothing happens at the boundaries between s_i and the FOV (for a period of time), which is a *null* event. Denoting these events e_e, e_x, and e_n, respectively, the collection of possible FOV events for a shadow s_i is the set

$$E_{\mathrm{FOV}} = \{e_e, e_x, e_n\}.$$

Some sensors may only detect the enter and exit events explicitly, such as a sensing node in a sensor network that only senses targets passing through the boundary of its sensing range. For detection beams, the FOV is a line segment, which causes two FOV events to happen consecutively (see Fig. 6). Certain systems may not have FOV events at all; an instance is a PE game in which the evader always avoids appearing in the pursuer's FOV.

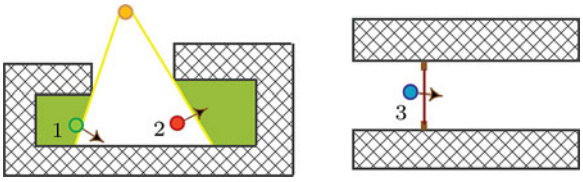

Fig. 6. FOV events (left) for an environment with obstructed visibility and for (right) an environment with detection beams. 1) A target is about to exit a shadow into the FOV of the sensor (yellow disk). 2) A target is about to enter a shadow from the sensor's FOV. 3) A target is about to enter and exit the FOV of a beam sensor.

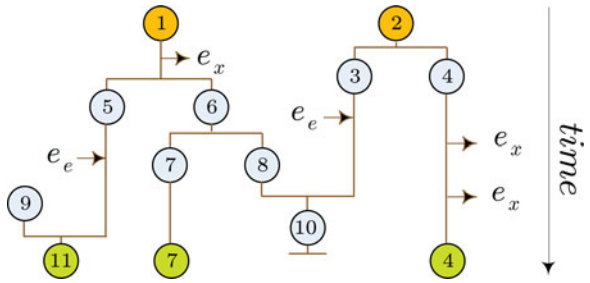

Fig. 7. Typical sequence of critical events. The circles with numbers represent the shadows; the labeled arrows associate FOV events to shadows.

The game ends when an evader is found or when it is confirmed that no evader is in the environment.

Since component events and FOV events both happen as robots move along some path τ in the free space F, it makes sense to treat them as a whole. It does not take much to represent them together: We can simply augment the shadow sequence to include the FOV events. A typical combined sequence of critical events is shown in Fig. 7. To incorporate FOV events, the invariance from Observation 1 needs to be updated.

Observation 2: In an environment with component and FOV events, the number of targets hidden in a workspace-time shadow is invariant between FOV events (excluding null events) associated with the shadow; the time span of such invariance is again maximal.

To see why the previous statement is true, note that an enter FOV event can be viewed as an appear component event immediately followed by a merge component event. Same breakdown holds for exit FOV events. The case is, then, reduced to Observation 1. Observation 2 establishes that for the task of tracking hidden targets that move continuously, any sensor data that are unrelated to critical events can be safety discarded without adverse effects.

C. Problem of Tracking Hidden Targets

With the introduction of component and FOV events, we can formally define the general problem of tracking hidden targets that move continuously. The following inputs are assumed: 1) an initial distribution of targets (in shadows) whose total number remains invariant; 2) an ordered sequence of component and FOV events for the time interval $[t_0, t_f]$; and 3) any target motion dynamics (e.g., nondeterministic) that may provide additional information about critical events.

From these inputs, the task is to track the evolution of the target distribution and, in particular, to estimate at $t = t_f$ the possible number of targets in a given set of shadows. For the rest of this paper, we focus on two aspects of this problem: 1) a nondeterministic setting in which targets move nondeterministically but critical events are observed without error and 2) a probabilistic setting in which the targets' movement has a probabilistic model and there are imperfect sensors.

IV. Tracking Nondeterministically Moving Targets: The Formulation and an Integer Linear Programming Perspective

A. Problem Formulation

In the *nondeterministic* setting, we assume that the targets move nondeterministically. In particular, when a shadow s_i splits into shadows s_j, s_k, the targets inside s_i can split in any possible way as long as the numbers of targets in s_j and s_k are both nonnegative. The component events and FOV events are assumed to be observed without error. Given such assumptions, the observation history can be partitioned into two inputs to our filter algorithm: 1) a sequence of shadow and FOV events and 2) the initial conditions of targets in the shadows at time $t = t_0$. A typical initial condition for a shadow takes the form

$$\{(a_1, l_1, u_1), (a_2, l_2, u_2), \ldots, (a_k, l_k, u_k)\} \tag{1}$$

where a_i denotes a subset of target attributes (such as having red color). We assume that elements of the set $\{a_i\}$ for a shadow are pairwise disjoint: If a_i has red color, then no $a_j, j \neq i$ can include targets with the attribute of having red color. The corresponding l_i and u_i denote the lower and upper bounds on the number of targets in the shadow with attribute a_i. For example, we may know that at the beginning, a shadow have six to nine green targets and five targets that may be blue or red. In this case, the initial condition can be written as $\{(c = \text{green}, 6, 9), (c = \text{blue or red}, 5, 5)\}$.

With these inputs, the main task is to determine the lower and upper bounds on the number of targets in any given set of shadows at $t = t_f$ for any combinations of attributes. These obtained bounds are always tight in the sense that any target distribution falling in these bounds is a possible outcome given the initial condition and the observation history.

To make the explanation of the algorithm clear, we first work with a single attribute and ignore FOV events. We also assume for the moment that the initial conditions are tight in the sense that all possible choices of values must be consistent with the later observations (e.g., we cannot have a initial condition of four to six targets in a shadow and later find that it is only possible to have two targets in it). We will then show how FOV events, multiple attributes, and other extensions can be handled incrementally.

B. Integer Linear Programming Perspective

For the simplest case, since there is a single attribute and the FOV events are ignored, we can represent the number of targets in a shadow with a single unknown quantity. Let the set of

shadows be $\{s_i\}$; we denote the set of corresponding unknowns as $\{x_i\}$. We can write the initial condition for each shadow at $t = t_0$ as two constraints

$$l_i \leq x_i \leq u_i. \tag{2}$$

For each event in the sequence of component events, we then obtain one extra constraint of the following form:

$$\begin{aligned} &\text{Appear or disappear:} && x_i = d_i \\ &\text{Split or merge:} && x_i = x_j + x_k. \end{aligned} \tag{3}$$

Here, we allow that as an appear event happens, d_i targets may hide in s_i at the same time. This is more general than letting $d_i = 0$. To unify notation, we write these in the same way as the initial conditions by letting $l_i = u_i = d_i$. The same applies to the disappear events. Additionally, we have, for each shadow s_i, the constraint

$$x_i \geq 0. \tag{4}$$

Finally, the task becomes finding the lower and upper bounds of targets for a set of shadows at time $t = t_f$ indexed by $\mathcal{I}$. For the upper bound, we can write the problem as maximizing the sum of the set of unknowns

$$\text{maximize} \sum_{i \in \mathcal{I}} x_i. \tag{5}$$

Finding the lower bound, then, becomes maximizing the set of unknowns not indexed by $\mathcal{I}$ because the total number of targets are preserved. We have obtained an ILP problem: All critical events can be expressed using constraints of forms from (2)–(4), with the objective function having the form from (5). For example, if we are to express the ILP problem in the *canonical form*, all we need to do is to split each equality constraint [given by (3)] into two inequality constraints (e.g., $x_i = d_i$ becomes $x_i \leq d_i$ and $x_i \geq d_i$) and multiply all inequality constraints with -1 where necessary ($x_i \leq d_i \Rightarrow -x_i \geq -d_i$). This gives us the ILP problem in canonical form

$$\text{minimize} \sum_{i \in \mathcal{I}} -x_i, \quad \text{subject to } Ax \geq b, x \geq 0 \tag{6}$$

where A is the constraint coefficient matrix accumulated from initial condition and the critical events; x is the vector of unknowns (one for each shadow). The size of A is determined by the number of shadows and the number of critical events. For additional discussion on ILP modeling, see [30].

C. Polynomial Time Solvability of the Integer Linear Programming Problem

It is well known that the class of ILP problems is NP-complete in general. It turns out, however, that our ILP problem is not only feasible, but efficiently solvable as well. We point out that an actual target tracking problem may require solving more than a pair (upper and lower bounds) of ILP problems, as formulated in (6). For example, in a fire rescue scenario, it may be necessary to estimate upper and lower bounds on all current shadows individually. Nevertheless, as long as the number of ILP problems are manageable (say, linear with respect to the size of the inputs), the overall problem can also be efficiently solved, as we now show.

Lemma 3: The matrix A in (6) is totally unimodular.[1]

Proof: We use induction over the size of square submatrices of A to prove that all such submatrices must have determinant 0 or ± 1. As the base case, every element of A is 0 or ± 1. Suppose that all square submatrices of order n have determinant $0, \pm 1$. Denote these matrices $\mathcal{M}_n$. Suppose there is a square submatrix M of A of order $(n+1)$ with determinant not in $\{0, \pm 1\}$. Every constraint arising from (2)–(4), except for $x_i = x_j + x_k$, introduces rows in A with a single ± 1 in them; the rest of the row contains only 0s. If M contains a row arising from these types of constraint, then M must have determinant $0, \pm 1$ by induction. Suppose not. In this case, all rows of M are introduced by constraint of type $x_i = x_j + x_k$. Each such constraint brings in two rows of A with opposite signs and, therefore, cannot both appear in M. We can assume that M's first row has coefficients coming from one of the rows introduced by a split event, $x_i = x_j + x_k$. As a first case, let the i, j, kth columns of A correspond to i', j', k'th columns of M, respectively. To make M's determinant not in $\{0, \pm 1\}$, there needs to be another row in M that contains exactly two nonzero elements among i', j', k'th columns. This is only possible if s_j and s_k merge again, giving a constraint of the form $x_j + x_k = x_l$. We may let this row be the second row in M. This suggests that j', k'th column of M are all zeros after the second row; but this gives us that M has determinant 0. The second case is that M includes only two columns of A's i, j, kth columns. It can be checked, similarly, that M must have determinant 0. ■

Proposition 4: A polynomial time algorithm exists for the system described by (6).

Proof of Proposition 4: When the constraint matrix A is totally unimodular and b is a vector of integers, the minimal faces of the constraint polytope must assume integer coordinates, making the solution of the relaxed linear programming (LP) problem also the solution to the original ILP problem [36]. It is clear that b in (6) is integer. Lemma 3 gives us that A is totally unimodular. Therefore, a polynomial time algorithm such as interior point method can be applied to solve (6). ■

V. Tracking Nondeterministically Moving Targets: An Information Space Perspective and Efficient Algorithms via Combinatorial Filters

Although Proposition 4 tells us that the nondeterministic formulation can be solved in polynomial time using generic LP algorithms, it is not clear that these algorithms fully explore the intrinsic structure of the problem at hand. In this section, we briefly review the *information space* (I-space for short; see [22], ch. 12] for an introduction) and show how the I-space framework can help with the systematic exploration of the structure of filtering problems that are combinatorial in nature. For our particular problem, we show that additional information can be discarded from the shadow sequence to yield a further condensed

[1] An integer square matrix A is unimodular if $\det A = \pm 1$. A matrix B is totally unimodular if every non-singular square submatrix of B is unimodular.

information state (I-state). Algorithmic solutions based on max-flow are then introduced, followed by various extensions.

A. Information Space as a Guiding Principle for Task-Based Data Filtering

As a shadow sequence is extracted from an observation history, a much condensed combinatorial structure is left. This choice is not arbitrary: The general task of tracking unpredictable targets outside the sensor range induces an equivalence relation over the workspace-time space that yields the space of shadows; the evolution of these shadows then gives rise to a space of shadow sequences. In this section, we review I-space/I-state concepts and explain how shadow sequences can be viewed as *derived* I-states and the space formed by them a *derived* I-space. We also characterize how I-spaces/I-states, tasks, and filters are closely related.

For any problem, I-space analysis begins with the *history I-space*, i.e., $\mathcal{I}_{\text{hist}}$, which is essentially the set of all data that robots may ever obtain. Formally, for a time period $[t_0, t_f] \subset T$, a perfect description of everything that occurred would be a *state trajectory* $\tilde{x}_t : [t_0, t_f] \rightarrow X$, where X is the combined state space of robots and targets. It is impossible to obtain this because not all target positions are known. What is available is the robots' trajectory $\tilde{q}_t = \tau$ and the sensor *observation history* $\tilde{y}_t : [t_0, t_f] \rightarrow Y$, which is produced by a sensor mapping $h : X \rightarrow Y$, in which Y is the observation space of the sensors. Let the robots also have access to some initial information η_0 at $t = t_0$. The *history I-state* at time, i.e., t, $\eta_t = (\eta_0, \tilde{q}_t, \tilde{y}_t)$, represents all information available to the robots. The *history I-space* $\mathcal{I}_{\text{hist}}$ is the set of all possible history I-states. $\mathcal{I}_{\text{hist}}$ is an unwieldy space; it must be greatly reduced if we expect to solve interesting problems. Imagine a robot equipped with a GPS and a video camera moves along some path τ. Without a specific task, the robot will not be able to decide what information it gathers is useful; therefore, it has to store all of $\tilde{q}_t, \tilde{y}_t$. Even at a relatively low spatial resolution and a frequency of 30 Hz, just keeping the robot's locations and the camera's images in compressed form requires a large amount of storage space, which presently is not generally possible over a long time period.

Once a task is fixed, however, it may become possible to reduce $\mathcal{I}_{\text{hist}}$ dramatically. For our specific task of tracking hidden targets in shadows, as we have established in Observation 2, all we need to know is the initial distribution of targets, the component events, and the FOV events. Since targets move unpredictably, other information contained in η_t does not help: the robots' exact location, the shape of the workspace shadows, and what the targets in the FOV are doing are not relevant. Thus, Observation 2 allows us to construct a *derived I-space* $\mathcal{I}_{ss}$, called the *shadow sequence I-space* that discards the irrelevant information. Consider the information contained in $\eta_t = (\eta_0, \tilde{q}_t, \tilde{y}_t)$. To derive $\mathcal{I}_{ss}$, the following reductions are made over $\eta_0, \tilde{q}_t$, and $\tilde{y}_t$.

1) The initial distribution of targets is extracted from η_0.
2) The shadow sequence is extracted via processing $\tilde{q}_t$ and $\tilde{y}_t$.
3) The observation history $\tilde{y}_t$ is compressed so that only critical events and temporal order between these events need to be recorded.

The result from this reduction is the *shadow sequence I-state* η'_t (Fig. 7 gives an example) that *lives* in $\mathcal{I}_{ss}$. $\mathcal{I}_{ss}$, as a complete yet more compact representation, immediately reveals much more structure that is intrinsic to our task than $\mathcal{I}_{\text{hist}}$ does. From this, we observe a general pattern that we exploit: Given $\mathcal{I}_{\text{hist}}$ and a task, we try to find one or more sufficient derived I-spaces and work exclusively in these derived I-spaces. In signal processing, a filter is defined as a device or process that removes from a signal unwanted features [19]. In this sense, the process of extracting shadows from $\tilde{q}_t$ and $\tilde{y}_t$ is exactly a filter. Moreover, $\mathcal{I}_{\text{hist}}$ and $\mathcal{I}_{ss}$ are connected through this filter. From this perspective, solving a task becomes finding the correct I-space, applying the associated filter, and performing additional computation as events happen. For the nondeterministic formulation, we call such filters *combinatorial filters*.

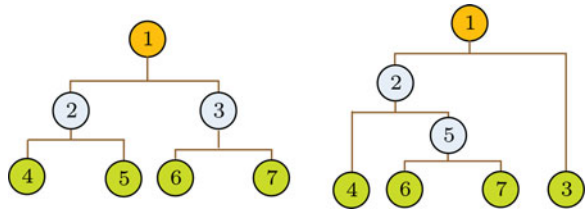

Fig. 8. Two shadow sequences that are equivalent for task of estimating lower and upper bounds on the number of targets in the shadows at time $t = t_f$.

B. Bipartite I-Space

As mentioned earlier, generic LP algorithms may not explore the full structure of our problem. One interesting property of our problem is that the distribution of targets in the shadows mimics network commodity flow. Another intrinsic and key property of our problem is that, in many cases, the relative order of component events does not affect the possible target distribution in the shadows. For example, the two shadow sequences in Fig. 8 are equivalent: The set of shadows at $t = t_f$ are basically the same. This allows us to safely discard the intermediate shadows to obtain a more compact I-space $\mathcal{I}_{\text{bip}}$, the *bipartite I-space*. The basic idea behind compressing $\mathcal{I}_{ss}$ into $\mathcal{I}_{\text{bip}}$ is that, since the robots' sensors cannot obtain information from the shadows as the robots move around, the information that really matters is how shadows from the beginning and the current time are related, while discarding the shadows from intermediate times. By conservation of targets in the environment, the number of targets in the shadows at $t = t_0$ and appeared shadows must be equal that in the shadows at $t = t_f$ and disappeared shadows. This hints toward a bipartite graph structure, which is why we denote the space of such I-states the bipartite I-space. To do the filtering, the component events are processed individually according to the procedure shown in Fig. 9. By the construction of $\mathcal{I}_{ss}$ and $\mathcal{I}_{\text{bip}}$, we have shown that $\mathcal{I}_{\text{hist}}, \mathcal{I}_{ss}$, and $\mathcal{I}_{\text{bip}}$ describe the same ILP problem:

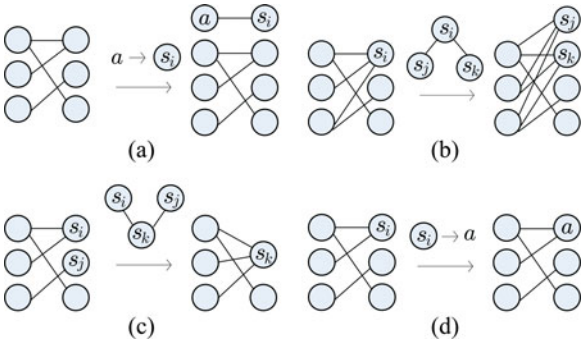

Fig. 9. Incrementally computing I-states in $\mathcal{I}_{\text{bip}}$. (a) Appear component event in which a targets goes into shadow s_i adds two vertices and an edge, with a associated with the left vertex. (b) Split event splits a vertex and all edges pointing to that vertex. (c) Merge event collapses two vertices into one and collapses their ingoing edges. (d) Disappear event in which s_i is revealed to have a targets in it only associates a with the vertex on the right side.

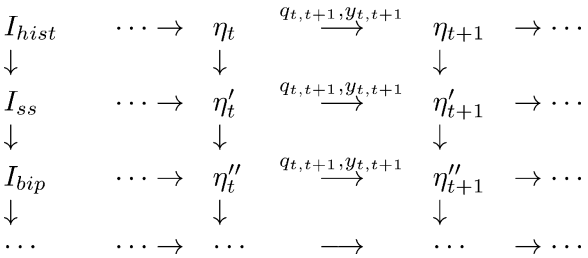

Fig. 10. Although it is possible to obtain $\eta'_{t+1} \in \mathcal{I}_{ss}$ from $\eta_{t+1} \in \mathcal{I}_{\text{hist}}$, it is also possible to derive it from η'_t and $q_{t,t+1}, y_{t,t+1}$, which also holds for $\eta''_{t+1} \in \mathcal{I}_{\text{bip}}$.

Proposition 5 Given that targets move nondeterministically, information from $\mathcal{I}_{\text{hist}}$ and the corresponding $\mathcal{I}_{ss}, \mathcal{I}_{\text{bip}}$ describe the same ILP problem of form (6).

Proof: The invariance from Observation 2 gives us that $\mathcal{I}_{\text{hist}}$ and $\mathcal{I}_{ss}$ are equivalent in capturing the distribution of hidden targets. To see that $\mathcal{I}_{ss}$ and $\mathcal{I}_{\text{bip}}$ are equivalent, we may consider each hidden target individually: Any flow of a target along a shadow sequence is possible in the corresponding bipartite structure, by construction. ■

A graphical illustration of relationship between I-spaces and I-states, which summarizes the I-space discussion, is given in Fig. 10. We point out that such hierarchical structures exist regardless of whether the formulation is nondeterministic or probabilistic; it so happens that for our filtering problem, the nondeterministic formulation leads to one more level of natural structure than the probabilistic formulation (see Section VI)

C. Tracking Targets as a Max-Flow Problem

With the bipartite I-state structure, we are ready to illustrate the complete combinatorial filtering process with a concrete example (the procedure was first introduced in [51]). After obtaining the bipartite structure, the rest of the algorithm is nothing more than applying a maximum flow subroutine (such as Edmonds–Karp) [10]. For the environment given in Fig. 11(a), a visibility cell decomposition procedure [6] will give us the shadow sequence I-state in Fig. 11(b). Applying the $\mathcal{I}_{\text{bip}}$ filter

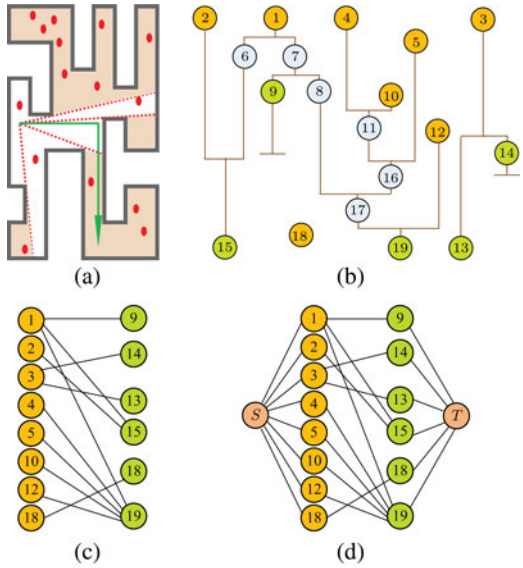

Fig. 11. (a) Two-dimensional office like environment. A single robot follows the green path. Red dots are illustrations of possible targets in the environment. (b) Shadow sequence I-state for the environment and path. The orange indexed shadows are these at $t = t_0$ or appearing; the green ones are these at $t = t_f$ or disappearing. Shadow s_{18} are both appearing and existing at $t = t_f$. (c) Bipartite I-state. (d) Augmented graph for running max-flow algorithm.

then gives us the bipartite graph in Fig. 11(c). Note that each shadow becomes a vertex (sometimes two vertices) of the bipartite graph. Once the bipartite graph is constructed, the task of determining lower and upper bounds on shadows at $t = t_f$ can be transformed into a max-flow problem. To achieve this, we first augment the graph by adding a source vertex S and sink vertex T. An edge is added between S and each shadow at $t = t_0$, as well as each appeared shadow, and an edge is added between T and each shadow at $t = t_f$, as well as each disappeared shadow. The end result of doing this to the graph in Fig. 11(c) is Fig. 11(d).

After obtaining the extended graph, capacities need to be assigned to edges of the graph before running max-flow. Let $e(v_1, v_2)$ be an edge in the graph from vertex v_1 to vertex v_2, and denote the capacity and flow on the edge as $c(v_1, v_2), f(v_1, v_2)$, respectively. Suppose that we want to obtain the upper bound on the number of targets in shadow s_{19}. The edges of the original bipartite graph will always have infinite capacities, which we will not mention again. For each edge between S and a shadow indexed i, let $c(S, i) = u_i$. In our example, these indices are 1–5, 10, 12, and 18. For each edge between a disappearing shadow indexed i, and T, let $c(i, T) = l_i$. These are 9 and 14 in our example. Since we want as many targets to go to s_{19} as possible, we let $c(i, T) = 0$ for $i = 13, 15, 18$ and $c(19, T) = +\infty$. After running the max-flow algorithm, the maximum possible number of targets that can end up in s_{19} is given by

$$f(19, T) + \sum_i f(i, T) - \sum_i c(i, T) \tag{7}$$

in which the summations are over indices of disappearing shadows. We need to consider disappearing shadows, since these shadows should have flow equal to their capacity, which is not

guaranteed by a max-flow algorithm. Filling in numbers into this example, assuming that the input lower/upper bound pairs for shadows 1–5, 9, 10, 12, 14, 18 are (2, 4), (0, 3), (5, 5), (2, 6), (4, 5), (2, 3), (1, 3), (3, 8), (2, 4), (5, 7), respectively, then, (7) gives us that shadow 19 can have at most 24 targets. One possible set of flow values yielding this results is $f(9,T) = f(14,T) = 2, f(13,T) = f(15,T) = 0, f(18,T) = 7$, and $f(19,T) = 24$. If we instead want the lower bound on the number of targets in s_{19}, we should let $c(S,i) = l_i$, $c(i,T) = l_i$ for $i = 9, 14$, $c(i,T) = +\infty$ for $i = 13, 15, 18$, and $c(19,T) = 0$. After running the max-flow algorithm, s_{19}'s lower bound is given by

$$\sum_i c(S,i) - \sum_j f(j,T) \tag{8}$$

in which the first summation is over all shadows connected to S, and the second summation is over all shadows connected to T. Using the earlier numbers, this minimum is 10 for shadow 19. A possible set of flow values yielding this is $f(9,T) = f(14,T) = f(15,T) = 1, f(13,T) = 4$, and $f(18,T) = 5$. The same procedure applies to an arbitrary set of shadows.

D. Incorporating Field-of-View Events

In the nondeterministic setting, there is no null FOV event. As mentioned in Observation 2, exit and enter FOV events can be handled by converting them into component events. To convert an enter FOV event of shadow s_i into component events, we simply create an appear component event of a single target and, then, merge the newly created shadow into s_i. Similarly, an exit FOV event can be converted into a split component event followed by a disappear component event. The rest of the algorithm stays the same. The problem is, however, if there is a large number of FOV events compared with the number of component events, this approach will slow down later steps of the algorithm, since it will create two component events per FOV event. Fortunately, there is no reason to handle each FOV event individually; since each FOV event is associated with some shadow, we can group them based on this association. The only caveat is that we cannot just group all FOV events for one shadow into a single *batch* FOV event as this can introduce information loss. For example, if $e_x, e_x, e_e,$ and e_e happens to shadow s_i, this is not equivalent to nothing has happened: We know that s_i must have at least two targets in it originally (a "surplus"). On the other hand, the just mentioned surplus and net target flow are the only two pieces of information that FOV events of a shadow give us; hence, up to two batch FOV events can summarize all information contained in all FOV events for a given shadow. Let $\langle e_j \rangle$ be the sequence of FOV events for a shadow s_i in which e_j is either e_e or e_x; we build a counter to track the surplus of s_i as $d_{\min} = \min\{d_j\}$, where d_j is defined as

$$d_j = \begin{cases} d_{j-1} + 1, & \text{if } e_j = e_e \\ d_{j-1} - 1, & \text{if } e_j = e_x \\ 0, & \text{if } j = 0. \end{cases}$$

Let d_{tot} be d_j for the last j, i.e., the net target flow from FOV events. We have four cases. If $d_{\min} = d_{\text{tot}} = 0$, we do nothing. If $d_{\min} \geq 0$ and $d_{\text{tot}} > 0$, we only need to create one batch enter FOV event for s_i with d_{tot} number of targets. If $d_{\min} < 0$ and $d_{\text{tot}} = d_{\min}$, we only need to create one batch exit FOV event with $|d_{\min}|$ number of targets. In the last case, we need to create one batch exit FOV event with $|d_{\min}|$ number of targets and, then, an enter FOV event with $d_{\text{tot}} - d_{\min}$ number of targets. We can, then, apply the naive approach from the beginning of this section to convert these batch FOV events into component events. With this construction, we never need to handle more than $5n$ events, where n is the maximum number of shadows.

E. Solving a Variety of Other Tasks

The ability to obtain lower and upper bounds of the number of targets hiding inside a shadow easily extends to other useful tasks. We briefly cover a few of these variations.

Refining initial bounds: Max-flow computations can also be used to refine the lower and upper bounds from initial conditions if they are not tight. To get a refined lower bound for a shadow at $t = t_0$, say s_1 from Fig. 11(b), let $c(S,1) = l_1$, $c(S,i) = u_i$ for $i \neq 1$, $c(i,T) = u_i$ for disappearing shadows, and $c(i,T) = 0$ for the rest. After running max-flow on this network, a tighter lower bound, if there is one, is given by

$$l_1' = l_1 + \sum_i c(i,T) - \sum_j f(j,T). \tag{9}$$

The summations are done similar to that of (8). To refine u_1, let $c(S,1) = u_1$, $c(S,i) = l_i$ for $i \neq 1$, $c(i,T) = u_i$ for disappearing shadows and $c(i,T) = +\infty$. After running max-flow

$$u_1' = f(S,1). \tag{10}$$

This procedure also applies to a set of shadows.

Counting: In this case, the total number of targets, i.e., n, is unknown. For determining n, the lower and upper bounds on each shadow at $t = t_0$ are set as $l_i = 0, u_i = +\infty$. As new component or FOV events are observed by the robots moving in the environment, the previous procedure is run to keep refining the initial bounds. Once we have $l_i = u_i$ for each initial condition, n has been determined. Note that if the free space is not completely explored, then the upper bound remains at infinity. Another instance of counting is knowing n. For example, in a wild animal preserve, it may be required that the total number of a species is verified periodically. This reduces to the problem of being given n and wanting to account for all of them. To verify the count, we can keep track of the lower bounds on the total number of targets, and if the number agrees with n, then the task has been accomplished.

PE: Suppose there is a single evader and the task is to determine where it might be. In this case, $l_i = 0$ and $u_i = 1$ for each shadow at $t = t_0$. There are three possibilities for each shadow at $t = t_f$: 1) $l_i = u_i = 0$ (the evader is not in s_i); 2) $l_i = u_i = 1$ (the evader is definitely in s_i); and 3) $l_i = 0, u_i = 1$ (the evader may or may not be in s_i). Note that this is a passive version of the PE problem. We do not determine a trajectory that is guaranteed to detect the evader. In general, this problem is NP-hard [14]. Nevertheless, the calculation method that is proposed in this

paper can be used with heuristic search techniques (or even human operators) to correctly maintain the status of the pursuit.

F. Incorporating Distinguishability

So far, we only considered the case of a single attribute, which is the fully indistinguishable case. What about multiple attributes? We consider two important cases of distinguishability based on whether attributes get mixed up or not. If attributes are not intertwined, i.e., each a_i in (1) is a single attribute, it is straightforward to see that for m attributes, all we need to do is to run the algorithm for a single attribute m times, once for each attribute. Additional computation can, then, be performed to calculate more complicated combinations. For example, if we want the lower and upper bounds on the number of all targets for a shadow, then we can simply add up individual lower and upper bounds.

For the second case in which we may have multiple attributes for some a_i, the aforementioned approach does not work. Using the example from Fig. 11, suppose that there are two teams, i.e., red and blue, and the initial conditions of shadows at $t = t_0$ are of the form (red or blue, l_i, u_i). Suppose that we want to get the lower and upper bounds of the number of targets in s_{19} again. For lower bounds, four computations are needed: first, we set red capacities to 0 and blue capacities to l_i for all edges starting from S. The capacities for each color for edges ending in T are set as earlier. Running two max-flow computations, i.e., one for red and one for blue, gives us one possible lower bound l_{r1}, l_{b1}. Switching red and blue and repeat the aforementioned procedure gives us another lower bound l_{r2}, l_{b2}. We should have $l_{r1} + l_{b1} = l_{r2} + l_{b2}$. The lower bound on s_{19} is then $l_{r1} + l_{b1}$ red or blue targets with between l_{r1} and l_{r_2} red targets. The upper bound can be obtained similarly.

VI. Imperfect Sensors, Probabilistic Events, and Bayesian Filters

Now consider the case of *probabilistic* uncertainty. So far, we have assumed that shadows and events are always reported without any error, which is unrealistic in practice. For detecting shadows, we already mentioned that true sensing range may be unavailable for some sensors, and sometimes, it is simply computationally impractical to obtain the exact visible/shadow region. However, if we settle for partial correctness, then probabilistic models can be applied. For example, when we deal with sensor networks, conservative, probabilistic estimates of sensing range may suffice.

The same principle applies to FOV events. For each of the three FOV events, we assume that the sensors on the robots may correctly observe it or mistake it for the other two events. An enter event for a component may be reported by the sensor as an enter, exit, or null event; the same applies to exit and null events. That is, the sensor mapping is given by $h : E_{\mathrm{FOV}} \to Y_{\mathrm{FOV}}$, with Y_{FOV} being the set of FOV observations $Y_{\mathrm{FOV}} = \{y_e, y_x, y_n\}$, where y_e, y_x, and y_n are enter, exit, and null observations. The map h can be deterministic, nondeterministic, or probabilistic. In this section, the case of a probabilistic FOV event-sensor mapping is investigated, together with the assumption that the dynamics of a split event is provided.

Before moving on, we introduce some notations to facilitate the discussion of the probabilistic formulation. We use s_i to denote the shadow with label i, as well as the random variable for that shadow in the joint/multivariate distribution. For shadows $s_1, \ldots, s_n$, the joint distribution is then $P(s_1, \ldots, s_n)$, in which a specific entry is $P(s_1 = x_1, \ldots, s_n = x_n) \in [0, 1]$. In writing formulas and outlining algorithms, we shorten the repeated variables to "..." on both the left-hand side (LHS) and the right-hand side (RHS) of an expression. In such cases, the combined "..." on the LHS and RHS denote the same set of random variables. For example, $P(s_1, s_2, s_3, s_4) = P(s_1, s_2, s_k, s_3, s_4)$ is shortened to $P(\ldots) = P(\ldots, s_k, \ldots)$.

A. Problem Formulation

In the basic setup, besides the availability of a sequence of component and FOV event observations (see, e.g., Fig. 7), the following assumptions are made.

1) Component events are observed without error.
2) Targets are indistinguishable. The initial condition is given as a joint probability distribution $P(s_1, \ldots, s_n)$ of targets in the n shadows at $t = t_0$.
3) When a split component event happens, a probabilistic *split rule* decides how the targets should redistribute.
4) Observations of FOV events follows distribution given by $P(\mathbf{e} = e|\mathbf{y} = y), e \in E_{\mathrm{FOV}}, y \in Y_{\mathrm{FOV}}$.

After general algorithms are presented, we discuss extensions relaxing the first two assumptions. The last two assumptions can be satisfied by collecting and analyzing sensor data from the same environment; the necessity of these two assumptions will become self-evident shortly. Given these assumptions, we want to obtain the target distribution in the m shadows, $P(s'_1, \ldots, s'_m)$, at time $t = t_f$.

The resulting joint probability distribution is useful in solving many decision-making problems; for example, in a fire evacuation scenario, knowing the expected number of people trapped in various parts (shadows) of a building (possibly estimated through observations from infrared beam sensors or security cameras), firefighters can better decide which region of the building should be given priority when they look around. The expected number of people in each shadow is readily available from the joint probability distribution.

B. Processing Component Events

To understand how observations affect target distributions in a probabilistic setting, let us first look at the component events (we do not distinguish between events and observations for these, since they are the same by assumption). Among the four types of component events, split and disappear events are more important than appear and merge events.

1) Split: A split event introduces more uncertainty. As a shadow splits into two disjoint shadows, the probability masses in the newly spawned shadows cannot be predicted without additional information because the sensors cannot see what happens within the shadow region during a split event. The issue is

TABLE I
EXAMPLE OF A MERGE EVENT

before merge	$P(s_1 = 1, s_2 = 1, s_3 = 4) = 0.2$
	$P(s_1 = 1, s_2 = 2, s_3 = 3) = 0.2$
	$P(s_1 = 1, s_2 = 3, s_3 = 2) = 0.2$
	$P(s_1 = 2, s_2 = 1, s_3 = 3) = 0.2$
	$P(s_1 = 2, s_2 = 2, s_3 = 2) = 0.2$
after merge	$P(s_1 = 1, s_4 = 5) = 0.2 + 0.2 + 0.2 = 0.6$
	$P(s_1 = 2, s_4 = 4) = 0.2 + 0.2 = 0.4$

resolved by the introduction of a *split rule* that is obtained from supporting data or an oracle, which dictates how the originating shadow's probability mass should be redistributed. For example, statistical data may support that the number of targets in the child shadows are proportional to their respective areas.

2) Disappear: When a shadow disappears, the targets hiding behind it are revealed. This information can be used to update our belief about the target distribution by eliminating some improbable distributions of targets. In particular, it can reduce the uncertainty created by split events. For example, suppose that a shadow s_i, having d_i targets in it (with 100% probability), splits into shadows s_j and s_k. It is possible that s_j has 0 to d_i targets in it, as does s_k. However, if s_k later disappears to reveal d_k targets in it and no other events happen to s_j and s_k, then s_j must have exactly $d_i - d_k$ targets in it. In general, assuming that shadow s_k disappears with a target distribution $P(s_k)$, the update rule is given by

$$P'(s_1 = x_1, \ldots, s_n = x_n) \propto \sum P(s_1 = x_1, \ldots, s_k = x_k, \ldots, s_n = x_n) P(s_k = x_k)$$

in which the summation is over all joint probability entries of $P(s_1, \ldots, s_n)$ such that $s_k = x_k$. Normalization is required.

3) Appear: An appearing shadow s_k, with distribution $P(s_k)$, can be joined with the rest via combining the independent distributions $P(s_k)$ with $P(s_1, \ldots, s_n)$:

$$P'(s_1 = x_1, \ldots, s_n = x_n, s_k = x_k) = P(s_1 = x_1, \ldots, s_n = x_n) P(s_k = x_k).$$

4) Merge: In this case, two probability masses are collapsed. We simply collect the joint distribution to form a single one

$$P'(\ldots, s_k = x_k) = \sum_{x_i + x_j = x_k} P(\ldots, s_i = x_i, \ldots, s_j = x_j, \ldots)$$

where s_k is the merged shadow of shadows s_i and s_j. A detailed example is given in Table I in which the original shadows are $s_1, s_2,$ and s_3, and s_2, s_3 merge to form shadow s_4.

C. Processing Field-of-View Events and Observations

Shifting to FOV events, we observe that an enter event only affects the shadow being entered by increasing the expected number of targets in the shadow. If there is a single shadow s and an enter event happens, we merely update $P(s = d_i) = p_i$ to $P(s = d_i + 1) = p_i$. On the other hand, an exit event does the opposite, and we change $P(s = d_i) = p_i$ to $P(s = d_i - 1) = p_i$. A complication arises here: If shadow s_i splits into shadows s_j, s_k, and an e_x event happens to shadow s_j, it suggests that it is impossible for s_j to have 0 target before the e_x event. The affected probability mass needs to be removed and the remaining values renormalized. The null event does not change the target distribution.

Now, to propagate a probability mass through an FOV observation, i.e., y, we essentially break the entry into three pieces according to the aforementioned rules, multiplying each resulting entries with the probability $P(\mathbf{e} = e_e \mid \mathbf{y} = y)$, $P(\mathbf{e} = e_x \mid \mathbf{y} = y)$, and $P(\mathbf{e} = e_n \mid \mathbf{y} = y)$, respectively. If an enter event is not possible for the observation, the two remaining entries are renormalized.

D. Accurately Propagating Probability Masses

The first algorithm that we introduce in this section is one that solves the probabilistic formulation from Section VI-A exactly. As events happen, the probability mass, i.e., $P(s_1, \ldots, s_n)$, is updated according to Algorithms 1 and 2 based on earlier analysis, in which the *observation* data structure is defined in Table II.

Algorithm 1 PROCESSPROBABILITYMASS

Input: $P(s_1, \ldots, s_n)$, the initial target distribution
Q, the queue of observation sequences
a **split rule**
$P(\mathbf{e} \mid \mathbf{y})$, the sensor statistics
Output: the target distribution after all observations

foreach event *observation* o in Q
  switch($o.event$)
  case *appear*:
    update all $P(s_1 = x_1, \ldots, s_n = x_n) = p_j$ entries to
      $P(s_1 = x_1, \ldots, s_n = x_n, o.s_e = n_e) = p_j * P(o.s_e = n_e)$
  case *disappear*:
    set $P(s_1 = x_1, \ldots, s_n = x_n)$ to
      $\sum P(s_1 = x_1, \ldots, o.s_v = n_v, \ldots, s_n = x_n) * P(o.s_v = n_v)$
    remove stale entries and renormalize the probability masses
  case *split*:
    add two new shadows $o.s_{s1}$, $o.s_{s2}$
    split prob. mass in $o.s_s$ into $o.s_{s1}$, $o.s_{s2}$ by **split rule**
  case *merge*:
    add a new shadow $o.s_m$ and set $P(\ldots, o.s_m = n)$ to
      $\sum_{n_1+n_2=n} P(\ldots, o.s_{m1} = n_1, \ldots, o.s_{m2} = n_2, \ldots)$
  case *enter, exit, null*:
    call PROCESSFOVEVENT
return the updated target distribution

Algorithm 2 PROCESSFOVEVENT

Input: $P(s_1, \ldots, s_n)$, the target distribution
$P(\mathbf{e} \mid \mathbf{y})$, the sensor statistics
$y \in \{y_e, y_x, y_n\}$, the FOV observation
s_i, the affected shadow
Output: the target distribution after the observation

foreach $P(\ldots, s_i = x_i, \ldots) = p_j$ entry in the distribution
  let $P'(\ldots, s_i = x_i + 1, \ldots) = p_j * P(\mathbf{e} = e_e \mid \mathbf{y} = y)$
  let $P''(\ldots, s_i = x_i, \ldots) = p_j * P(\mathbf{e} = e_n \mid \mathbf{y} = y)$
  if $x_i > 0$
    let $P'''(\ldots, s_i = x_i - 1, \ldots) = p_j * P(\mathbf{e} = e_x \mid \mathbf{y} = y)$
  else
    normalize P', P'' such that $P' + P'' = p_j$
  remove $P(\ldots, s_i = j, \ldots) = p_j$ entry
  store entries P', P'' and P''' if applicable
return the updated target distribution

TABLE II
DATA STRUCTURES

observation data structure used in Algorithm 1

event	event type, can be one of *appear, disappear, split, merge* component events and *enter, exit, null* FOV events
s_s	the originating shadow in a split event
s_{s1}	the first new shadow after a split event
s_{s2}	the second new shadow in a split event
s_{m1}	the first shadow in a merge event
s_{m2}	the second shadow in a merge event
s_m	the newly merged shadow
s_e	the newly appeared shadow from an appear event
$P(s_e = n_e)$	probability that s_e contains n_e targets
s_v	the disappearing shadow in a disappear event
$P(s_v = n_v)$	probability that s_v contains n_v targets

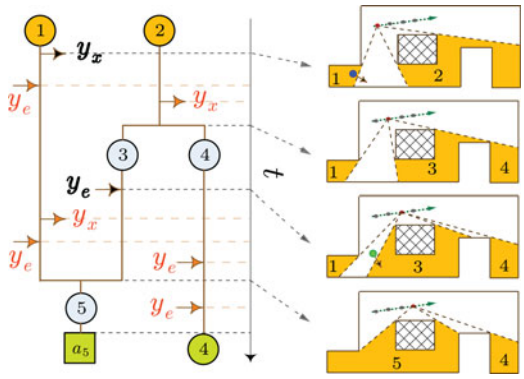

Fig. 12. Simple event observation sequence is generated (on the left, with only two FOV observations marked with bold faced font) when a robot carrying omnidirectional, infinite range sensor follows the dotted path in a polygonal environment with a hole (the four figures on the right). The last event, i.e., disappearing of shadow s_5, is not shown on the right; we note that additional resources are needed to make s_5 disappear (say, a subsearch team). A slightly more complicated sequence is also possible with six additional FOV observations (on the left, marked with lightened font).

As a demonstration, we work through the observation sequence given by Fig. 12, with the following assumptions: 1) Initially there are two targets each in shadow s_1, s_2; 2) the split rule is that each target has 0.5 probability of going into each of the two split shadows; 3) there is no null event or observation, with the true positive rate for any observation being $p = 0.9$; and 4) $a_5 = 1$ with probability 0.5 and $a_5 = 2$ with probability 0.5. The extra assumptions are made so that the calculation of the probability mass entries is limited and the entries can be listed in a table. The iterative processing of observations is shown in Table III. The distribution is represented using a table of joint probabilities, which is always practical when there are not too many targets and events. Renormalization is performed in the third step for the first and sixth entries, as well as in the last step. In the merge step, the third and seventh entries from previous step are combined, as are the fifth and ninth entries. A graphical illustration of the probability masses during each step of the run is given in Fig. 13. Note that the dimensions change as component events happen.

To verify the correctness of the outcome, Monte Carlo trials are also run, in which individual targets are propagated through the observation one by one. Since it is not an exact method, we leave the details of it to the next section. After 1000 successful

TABLE III
EXAMPLE OF THE EVOLUTION OF THE TARGET DISTRIBUTION THROUGH EVENT OBSERVATIONS

observation	probability masses
initial	$P(s_1 = 2, s_2 = 2) = 1$
y_x, s_1	$P(s_1 = 1, s_2 = 2) = 0.9$ $P(s_1 = 3, s_2 = 2) = 0.1$
split, $s_2 \rightarrow s_3, s_4$	$P(s_1 = 1, s_3 = 0, s_4 = 2) = 0.9 * 0.25 = 0.225$ $P(s_1 = 1, s_3 = 1, s_4 = 1) = 0.9 * 0.5 = 0.45$ $P(s_1 = 1, s_3 = 2, s_4 = 0) = 0.9 * 0.25 = 0.225$ $P(s_1 = 3, s_3 = 0, s_4 = 2) = 0.1 * 0.25 = 0.025$ $P(s_1 = 3, s_3 = 1, s_4 = 1) = 0.1 * 0.5 = 0.05$ $P(s_1 = 3, s_3 = 2, s_4 = 0) = 0.1 * 0.25 = 0.025$
y_e, s_3	$P(s_1 = 1, s_3 = 1, s_4 = 2) = 0.225$ $P(s_1 = 1, s_3 = 0, s_4 = 1) = 0.45 * 0.1 = 0.045$ $P(s_1 = 1, s_3 = 2, s_4 = 1) = 0.45 * 0.9 = 0.405$ $P(s_1 = 1, s_3 = 1, s_4 = 0) = 0.225 * 0.1 = 0.0225$ $P(s_1 = 1, s_3 = 3, s_4 = 0) = 0.225 * 0.9 = 0.2025$ $P(s_1 = 3, s_3 = 1, s_4 = 2) = 0.025$ $P(s_1 = 3, s_3 = 0, s_4 = 1) = 0.05 * 0.1 = 0.005$ $P(s_1 = 3, s_3 = 2, s_4 = 1) = 0.05 * 0.9 = 0.045$ $P(s_1 = 3, s_3 = 1, s_4 = 0) = 0.025 * 0.1 = 0.0025$ $P(s_1 = 3, s_3 = 3, s_4 = 0) = 0.025 * 0.9 = 0.0225$
merge, $s_1, s_3 \rightarrow s_5$	$P(s_4 = 2, s_5 = 2) = 0.225$ $P(s_4 = 1, s_5 = 1) = 0.045$ $P(s_4 = 1, s_5 = 3) = 0.405 + 0.005 = 0.41$ $P(s_4 = 0, s_5 = 2) = 0.0225$ $P(s_4 = 0, s_5 = 4) = 0.2025 + 0.0025 = 0.205$ $P(s_4 = 2, s_5 = 4) = 0.025$ $P(s_4 = 1, s_5 = 5) = 0.045$ $P(s_4 = 0, s_5 = 6) = 0.0225$
disappear, s_5	$P(s_4 = 0) = 0.0769$ $(= 0.0225 * 0.5/((0.0225 + 0.045 + 0.225) * 0.5)$ $P(s_4 = 1) = 0.1538$ $P(s_4 = 2) = 0.7692$

random trials (this is the number of trials used for all Monte Carlo simulations in this paper), we obtained $P(s_4 = 0) = 0.079$, $P(s_4 = 1) = 0.154$, and $P(s_4 = 2) = 0.767$, which matches closely the results of the exact algorithm.

E. Efficiently Propagating Probability Masses

Although the algorithm PROCESSPROBABILITYMASS is exact, its performance directly depends on the number of probability mass entries of a particular problem. When there are few targets and events, this is not a problem; but what if this is not the case? For a slightly more complicated event observation sequence (see Fig. 12), with five targets each in shadow s_1 and s_2 to start, 135 joint probability table entries are obtained before the merge step, as shown in Fig. 14. The probability mass entries increase rapidly because of the split events and the FOV events. For a split event, if the originating shadow contains n targets, the number of probability mass entries can multiply by up to a factor of $n + 1$. For FOV observations, each has certain probability to be enter, exit, and null events, which may cause the number of probability mass entries to triple in the worst case. Therefore, as the number of targets and events increase, the number of probability mass entries may grow exponentially. Since processing each observation requires going through all the entries, computation time will also explode, suggesting that the exact algorithm will not work efficiently. On the bright side, when a large number of probability mass entries are present,

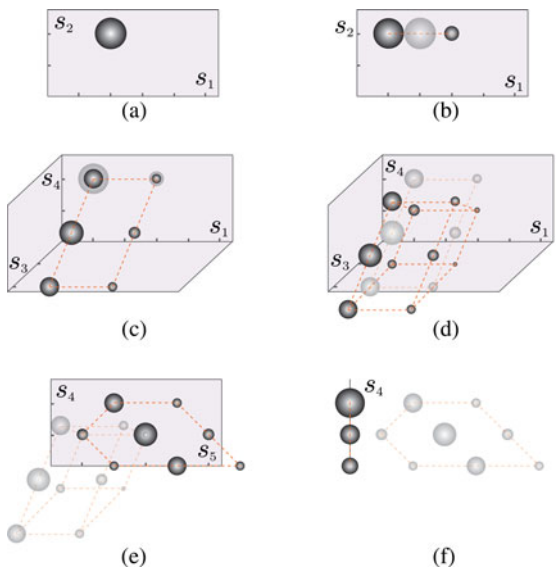

Fig. 13. Graphical display of the target probability mass as the algorithm ProcessProbabilityMass is run over the simple event observation sequence in Fig. 12. Each figure corresponds to one step in Table III. Lighter (if any) and darker balls represent probability masses before and after an event, respectively. The volumes are proportional to the magnitude of the probability mass entries.

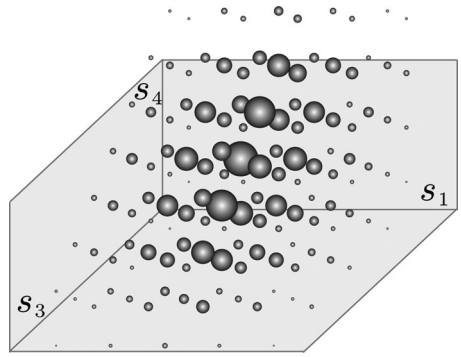

Fig. 14. Probability masses for the slightly more complicated observation sequence in Fig. 12 before shadows s_1, s_3 merge to form s_5. The axes s_1, s_3, and s_4, as shown in the figure, have ranges $[1, 9]$, $[0, 7]$, and $[0, 5]$, respectively, starting from the origin.

some of these entries must have very low weights; approximations become feasible.

Monte Carlo trials: Since our task is to probabilistically track targets, sequential Monte Carlo methods are a natural choice. As a first heuristic, we perform simple trials such that each trial starts with the initial distribution of targets. These targets are propagated through the event observations by querying a Monte Carlo simulator. During each trial, the outcome of simulation may contradict an observation, in which case the trial is simply discarded. After a certain number of successful trials are completed, the final target distribution is obtained. For example, the mean of the number of targets in a shadow at $t = t_f$ is simply the average of the number of targets in that shadow over all successful runs. For simulations in this paper, we require 1000 successful trials. Note that since the particular Monte Carlo simulation that we perform in this paper does not depend on data, its result is probabilistically correct and, therefore, can serve as baselines to verify results from other algorithms.

Improving the ProcessProbabilityMass algorithm: Observing that the computation is burdened by storing the sheer amount of probability mass entries when there are many targets and observations, an obvious simplification is to *resample* the entries and keep the important ones. For example, we may choose to retain the first 1000 probability mass entries of largest value. With each step of processing looking at each entry once, the processing time per step becomes a constant, albeit a large one. With this approximation, the earlier algorithm then runs in time *linear* in the number of observations. We call this heuristic *basic truncation*.

The problem with basic truncation, however, is that the trimmed away entries may turn out to be important. Take the processing in Table III; for example, if the fourth entry after the merge step, i.e., $P(s_4 = 0; s_5 = 2) = 0.0225$, is truncated, then the second entry in the end, i.e., $P(s_4 = 0) = 0.0769$, will be lost, which is significant. The issue becomes problematic very quickly as the number of coexisting shadows increases, since each shadow creates one dimension in the joint distribution, and sampling a high-dimensional space is inherently inefficient. To alleviate this problem, in addition to the basic truncation approach of keeping fixed amount of entries with highest probability after each update, we also employ the following.

1) Randomly allow probability mass entries with low value to survive truncation. In doing this, we hope to allow enough low probability yet important entries to survive truncation. We denote this heuristic as *random truncation*.
2) Retain more entries during update steps right before merge and disappear events. Since disappear events usually cause the number of probability mass entries to decrease dramatically, we can afford to keep more entries right before these events, without incurring much extra computational cost. Merge events also cause the number to decrease as some entries can be combined after merging. We combine this with random truncation and denote the resulting heuristic *random truncation with event lookahead*.

By construction, the additional heuristics do not incur more time complexity. There is a clear similarity between these heuristics and particle filtering: They all begin with a discrete set of probability masses, push the set through an update rule, and resample when necessary. They also share the same weakness: If the key sample points with low probabilities are truncated, the end result may be severely skewed. Unlike in typical particle filter problems, the number of random variables in our problem keeps changing with split and merge events.

F. Extensions

In Section VI-A, assumptions 1 and 2 are made to simplify the presentation of the probabilistic algorithms. The first assumption is that component events are observed without error, which is relatively straightforward to compensate if it fails to hold, at least in theory: All we need to do is to maintain a probability distribution over all possible sequence of shadows that are consistent with the robot's observations. Obtaining

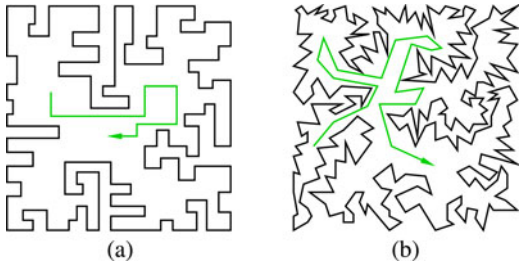

Fig. 15. Complicated examples that were used to test our approach. The given robot trajectories are shown as green lines in the direction of the arrow.

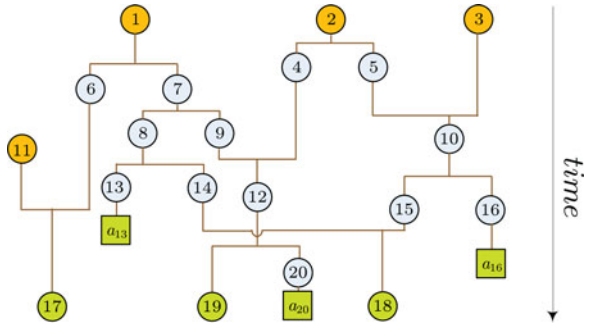

Fig. 16. Event observation sequence with a total of 20 shadows in its life cycle. The FOV observations are not marked.

expectations of the number of targets in any shadow can then be done by also calculating the expectation over all possible sequences of shadows that contain the target shadow. The computation effort will certainly increase; resampling can alleviate the burden somewhat.

Various distinguishability assumptions can be handled as well. Recall that in the nondeterministic formulation, two distinguishability cases are investigated. When there are only teams with single attributes, the approach from the nondeterministic setting applies by simply carrying out one computation per team. If the teams have multiple attributes (e.g., the initial condition may be given as a joint distribution of red and blue teams), a direct extension is performing one computation for each joint probability entries in the initial condition. This is clearly more work, and resampling may be necessary, depending on the granularity of the initial target distribution. On the plus side, although we lose some accuracy with resampling (to save computation time), a richer class of problems can now be handled because any initial condition can be described as a joint probability distribution.

VII. Simulation Results and Complexity Analysis

The simulation programs were developed adhering to the Java 1.6 language standard under the Eclipse environment. The computations were performed on a workstation with an Intel Core 2 Quad processor running at 3.0 GHz. The JavaVM has a maximum memory of 1.5 Gb.

A. Nondeterministically Moving Targets

For the nondeterministic case, we implemented and tested the algorithms for a single robot that moves in a simply connected polygonal region in $\mathbb{R}^2$ using an omnidirectional visibility sensor. We choose these environments, since efficient 2-D cell decomposition routines exist to allow us to continuously track the shadows. The setup also enables us to construct an oracle (not available to the algorithm) for distributing targets inside the free space to simulate their nondeterministic behavior. For max-flow, we implemented the $O(VE^2)$-time Edmonds-Karp max-flow algorithm [10], in which V and E are the numbers of vertices and edges in the flow graph, respectively.

For the environment in Fig. 15(a), the trajectory generates 85 component events. Our oracle randomly distributed 100 targets in the free space as the component events occur. This setting yields a bipartite graph that has 41 vertices and 60 edges. Calculating the lower and upper bounds for the 18 final shadows for a single team took 0.1 s. The second setup, which is shown in Fig. 15(b), has 385 component events, 491 total shadows, and 124 vertices in the bipartite graph with 339 edges. The example involves 1 million targets with five teams that intersperse. The bounds on the 12 final shadow components for all five teams were computed under 1 s.

The inputs to the base algorithm (single attribute, no FOV events) are the following: 1) a sequence of n shadows and 2) the initial condition which takes the form of a pair of lower and upper bounds for each shadow at $t = t_0$. In the worst case, there are $O(n)$ vertices and $O(n^2)$ edges in the bipartite graph. Edmonds–Karp max-flow, then, gives us $O(n^5)$ running time in the worst case. Applying a push-relabel algorithm with first-in-first-out vertex selection rule will cut the running time to $O(n^3)$ [13]. Adding FOV events does not increase time complexity asymptotically, as discussed in Section V-D. Adding partial distinguishability, on the other hand, will introduce another input parameter m, which is the number of teams, that contributes linearly to time complexity. The typical worst case running time for the nondeterministic case is then $O(n^3m)$. The number of targets in the system does not directly affect the performance.

B. Probabilistic Setup

For the probabilistic case, we ran a simulation with the observation sequence in Fig. 16. The sequence contains 14 component event observations. We also included 32 FOV events scattered along the sequence, which are not marked in the figure. Shadows 1, 2, 3, 11, 13, 16, and 20 are associated with 10, 7, 8, 9, 6, 9, and 4 targets (with probability 1), respectively. For performance measures, we look at the time for one run of the algorithm to complete, as well as the expectation (mean and standard deviation for randomized methods) of targets in individual shadows at the end (s_{17}, s_{18}, and s_{19}). When we randomly pick entries to keep, the time result is averaged over ten runs, and the accuracy is given in the form of mean and standard deviation. In our implementation, we also make the following choices: 1) For random truncation, the entries are kept based on their probability multiplied by a random number in $(0, 1)$; and 2) for event lookahead, we will not truncate the entries if there is a disappear event within the next four events or a merge

TABLE IV
SIMULATION RESULTS OF DIFFERENT PROBABILISTIC METHODS

heuristic	s_{17}	s_{18}	s_{19}	t(s)
none, precise	11.12	5.84	5.60	329.5
TR-10000	failure			
TR-20000	10.67	4.85	5.33	6.1
TR-50000	11.00	5.38	5.52	15.5
TR-100000	10.96	5.59	5.53	29.4
TR-200000	11.06	5.73	5.56	61.4
RT-10000	frequent failure			
RT-20000	11.38(0.20)	5.31(0.23)	5.67(0.20)	6.1
RT-50000	11.16(0.02)	5.36(0.03)	5.64(0.02)	14.6
RT-100000	11.03(0.01)	5.62(0.01)	5.56(0.01)	28.3
RT-LA-2000	frequent failure			
RT-LA-5000	11.32(1.30)	6.54(1.46)	5.28(1.28)	2.0
RT-LA-10000	11.17(0.56)	5.87(0.91)	5.02(0.48)	4.2
RT-LA-20000	11.62(0.26)	5.30(0.18)	5.57(0.16)	8.3
RT-LA-50000	11.32(0.01)	5.51(0.01)	5.60(0.01)	17.7
Monte Carlo	11.16	5.58	5.57	42.1

TABLE V
SIMULATION RESULTS OF SELECTED PROBABILISTIC METHODS OVER A LARGE PROBLEM INSTANCE

Heuristic	s_{17}	s_{18}	s_{19}	t(s)
none, exact	out of memory after 10 mins			
Monte Carlo	18.26	22.25	11.85	43.2
RT-100000	17.78(0.03)	21.83(0.03)	12.34(0.02)	66.3
RT-LA-50000	18.24(0.08)	21.99(0.07)	12.57(0.07)	40.6

event within the next two events. The outcome is summarized in Table IV. The heuristics basic truncation, random truncation, and random truncation with event lookahead are shortened as TR, RT, and RT-LA, respectively. The number following the method is the number of entries kept. By *frequent failure*, we mean that more than one third of the time, the heuristic fails to give a valid result. These are indicative of minimum number of entries needed for the method to work.

The result shows that when no heuristic is used, the algorithm takes much more time to finish. This is not surprising since the time complexity is induced by the space requirement for storing the probability mass entries. On the other hand, all of the truncation heuristics work reasonably well, with the randomized truncation plus event lookahead greatly reduces the number of entries to retain. The RT-LA-50000 run compares well with the TR-100 000 run on accuracy but uses one third less time. We expect the advantage to become more obvious as more targets are present in the system.

For a second test, we change the number of targets in shadows 1, 2, 3, 13, 16, and 20 to 25, 22, 23, 8, 15, and 9, while leaving other observations unchanged. With the increased number of targets, the basic algorithm runs out of memory after ten min, before the third split is completed. At the peak of its memory usage during the failed run, there are more than 2×10^7 probability mass entries. On the other hand, the randomized methods do not have this problem: Both RT-100 000 and RT-LA-50 000 yield good results, compared with Monte Carlo trials, with similar running time. The result is summarized in Table V. Comprehensive performance analysis of probabilistic algorithm is hard, since the performance depends on external factors, such as the implementation of the specific split rule, random number generator, and so on. Nevertheless, for completeness, we discuss the performance at a higher level. To avoid the issue of external factors, we assume that at each step, each probability mass takes constant time to process. Unlike the nondeterministic case, running time of the PROCESSPROBABILITYMASS algorithm may depend heavily on the number of targets in the system via the split rule. If there are n split events with an average number of targets in the originating shadow being p as well as n_f FOV events, with the reasonable additional assumption that merge, appear, and disappear events are on the same order as split events, the PROCESSPROBABILITYMASS algorithm can take time $O(p^n 3^{n_f})$. The running time of the resampling based algorithms has a big constant depending on the number of entries to keep but otherwise depends only linearly on the number of critical events.

VIII. CONCLUSION

In conclusion, we have formulated and solved, at a very general level, the problem of tracking targets moving in and out of the FOV of moving sensors. The resulting filters may be applied in numerous settings, such as PE, target enumeration, and situational awareness. When targets move nondeterministically, a combinatorial filter is proposed for the tracking task: We show that the naturally emerging ILP problem is, in fact, solvable in polynomial time and provide an efficient max-flow-based solution for it. For the probabilistic filtering problem in which targets move probabilistically and sensors are not reliable, we give both exact and efficient algorithms that handle the several possible scenarios, depending on the number of targets and observations in a system. In solving the more general, probabilistic version of the tracking problem, a clear link is also established between combinatorial filtering and Bayesian filtering methods: The final target distribution is in essence associating the combinatorial solution, i.e., a polytope structure, with appropriate probabilities. Viewing it from another angle, the probabilistic shadow I-space extends naturally from its nondeterministic counterpart by merely adding dimensions to record probabilities.

REFERENCES

[1] S. Alexander, R. Bishop, and R. Ghrist, "Pursuit and evasion in nonconvex domains of arbitrary dimension," in *Robotics: Science and Systems II*, G. S. Sukhatme, S. Schaal, W. Burgard, and D. Fox, Eds. Cambridge, MA: MIT Press, 2007.

[2] L. Alonso, A. S. Goldstein, and E. M. Reingold, "Lion and man: Upper and lower bounds," *ORSA J. Comput.*, vol. 4, no. 4, 1992.

[3] Y. Baryshnikov and R. Ghrist, "Target enumeration via euler characteristic integrals," *SIAM J. Appl. Math.*, vol. 70, no. 4, pp. 825–844, Aug. 2009.

[4] P. E. Berry, C. Pontecorvo, and D. A. B. Fogg, "Optimal search, location and tracking of surface maritime targets by a constellation of surveillance satellites," DSTO Inf. Sci. Lab., Edingburgh, SA, Tech. Rep. no. DSTO-TR-1480, 2003.

[5] S. D. Bopardikar, F. Bullo, and J. P. Hespanha, "On discrete-time pursuit-evasion games with sensing limitations," *IEEE Trans. Robot.*, vol. 24, no. 6, pp. 1429–1439, Dec. 2008.

[6] P. Bose, A. Lubiv, and J. I. Munro, "Efficient visibility queries in simple polygons," in *Proc. Can. Conf. Comput. Geometry*, 1992, pp. 23–28.

[7] F. Bourgault, T. Furukawa, and H. F. Durrant-Whyte, "Coordinated decentralized search for a lost target in a Bayesian world," in *Proc. IEEE/RSJ Int. Conf. Intell. Robots Syst.*, 2003, vol. 1, pp. 48–53.

[8] W.-P. Chin and S. Ntafos, "Optimum watchman routes," *Inf. Process. Lett.*, vol. 28, pp. 39–44, 1988.

[9] W.-P. Chin and S. Ntafos, "Optimum watchman routes in simple polygons," *Discrete Comput. Geometry*, vol. 6, pp. 9–31, 1991.

[10] J. Edmonds and R. M. Karp, "Theoretical improvements in algorithmic efficiency for network flow problems," *J. ACM*, vol. 19, no. 2, pp. 248–264, 1972.
[11] B. P. Gerkey, S. Thrun, and G. Gordon, "Visibility-based pursuit-evasion with limited field of view," *Int. J. Robot. Res.*, vol. 25, no. 4, pp. 299–322, 2006.
[12] B. Gfeller, M. Mihalak, S. Suri, E. Vicari, and P. Widmayer, "Counting targets with mobile sensors in an unknown environment," in *Lecture Notes Comput. Sci., Algosensors*, vol. 4837, 2008, pp. 32–45.
[13] A. V. Goldberg and R. E. Tarjan, "A new approach to the maximum flow problem," in *Proc. 18th Annu. ACM Symp. Theory Comput.*, 1986, pp. 136–146.
[14] L. J. Guibas, J.-C. Latombe, S. M. LaValle, D. Lin, and R. Motwani, "Visibility-based pursuit-evasion in a polygonal environment," *Int. J. Comput. Geometry Appl.*, vol. 9, no. 5, pp. 471–494, 1999.
[15] O. Hájek, *Pursuit Games*. New York: Academic, 1975.
[16] Y. Ho, A. E. Bryson, and S. Baron, "Differential games and optimal pursuit-evasion strategies," *IEEE Trans. Autom. Control*, vol. AC-10, no. 4, pp. 385–389, Oct. 1965.
[17] R. Isaacs, *Differential Games*. New York: Wiley, 1965.
[18] V. Isler, S. Kannan, and S. Khanna, "Randomized pursuit-evasion in a polygonal environment," *IEEE Trans. Robot.*, vol. 5, no. 21, pp. 864–875, Oct. 2005.
[19] R. E. Kalman, "A new approach to linear filtering and prediction problems," *Trans. ASME, J. Basic Eng.*, vol. 82, pp. 35–45, 1960.
[20] T. Kameda, M. Yamashita, and I. Suzuki, "On-line polygon search by a seven-state boundary 1-searcher," *IEEE Trans. Robot.*, vol. 22, no. 3, pp. 446–460, Jun. 2006.
[21] S. Kopparty and C. V. Ravishankar, "A framework for pursuit evasion games in R^n," *Inf. Process. Lett.*, vol. 96, no. 3, pp. 114–122, 2005.
[22] S. M. LaValle, *Planning Algorithms*. Cambridge, U.K.: Cambridge Univ. Press, 2006.
[23] S. M. LaValle and J. Hinrichsen, "Visibility-based pursuit-evasion: The case of curved environments," *IEEE Trans. Robot. Autom.*, vol. 17, no. 2, pp. 196–201, Apr. 2001.
[24] S. M. LaValle, D. Lin, L. J. Guibas, J.-C. Latombe, and R. Motwani, "Finding an unpredictable target in a workspace with obstacles," in *Proc. IEEE Int. Conf. Robot. Autom.*, 1997, pp. 737–742.
[25] S.-H. Lim, T. Furukawa, G. Dissanayake, and H. F. Durrant-Whyte, "A time-optimal control strategy for pursuit-evasion games problems," in *Proc. IEEE Int. Conf. Robot. Autom.*, 2004, pp. 3962–3967.
[26] R. Mahler, "Objective functions for Bayesian control-theoretic sensor management—II: MHC-like approximation," in *New Developments in Cooperative Control and Optimization*, S. Butenko, R. Murphey, and P. Paralos, Eds. Norwell, MA: Kluwer, 2003, pp. 273–316.
[27] J. O'Rourke, *Art Gallery Theorems and Algorithms*. New York: Oxford Univ. Press, 1987.
[28] J. O'Rourke, "Visibility," in *Handbook of Discrete and Computational Geometry*, J. E. Goodman and J. O'Rourke, Eds., 2nd ed. ed. New York: Chapman & Hall/CRC, 2004, pp. 643–663.
[29] M. Pachter, "Simple motion pursuit-evasion differential games," presented at the Mediterranean Conf. Control Autom., Lisbon, Portugal, Jul. 2002.
[30] C. H. Papadimitriou and K. J. Steiglitz, *Combinatorial Optimization: Algorithms and Complexity*. Englewood Cliffs, NJ: Prentice-Hall, 1982.
[31] S.-M. Park, J.-H. Lee, and K.-Y. Chwa, "Visibility-based pursuit-evasion in a polygonal region by a searcher," Dept. Comput Sci., Korea Advanced Inst. Sci. Technol., Seoul, Korea, Tech. Rep. CS/TR-2001-161, Jan. 2001.
[32] T. D. Parsons, "Pursuit-evasion in a graph," in *Theory and Application of Graphs*, Y. Alavi and D. R. Lick, Eds. Berlin, Germany: Springer-Verlag, 1976, pp. 426–441.
[33] S. Petitjean, D. Kriegman, and J. Ponce, "Computing exact aspect graphs of curved objects: Algebraic surfaces," *Int. J. Comput. Vis.*, vol. 9, pp. 231–255, Dec. 1992.
[34] M. Pocchiola and G. Vegter, "The visibility complex," *Int. J. Comput. Geometry Appl.*, vol. 6, no. 3, pp. 279–308, 1996.
[35] S. Sachs, S. Rajko, and S. M. LaValle, "Visibility-based pursuit-evasion in an unknown planar environment," *Int. J. Robot. Res.*, vol. 23, no. 1, pp. 3–26, Jan. 2004.
[36] A. Schrijver, *Combinatorial Optimization*. New York: Springer-Verlag, 2003.
[37] J. Sgall, "A solution of david gales lion and man problem," *Theoretical Comput. Sci.*, vol. 259, no. 1–2, pp. 663–670, 2001.
[38] T. Shermer, "Recent results in art galleries," *Proc. IEEE*, vol. 80, no. 9, pp. 1384–1399, Sep. 1992.
[39] B. Simov, G. Slutzki, and S. M. LaValle, "Pursuit-evasion using beam detection," in *Proc. IEEE Int. Conf. Robot. Autom.*, 2000, pp. 1657–1662.
[40] J. Singh, R. Kumar, U. Madhow, S. Suri, and R. Cagley, "Tracking multiple targets using binary proximity sensors," in *Proc. Inf. Process. Sensor Netw.*, 2007, pp. 529–538.
[41] L. D. Stone, *Theory of Optimal Search*. New York: Academic, 1975.
[42] I. Suzuki and M. Yamashita, "Searching for a mobile intruder in a polygonal region," *SIAM J. Comput.*, vol. 21, no. 5, pp. 863–888, Oct. 1992.
[43] B. Tovar, F. Cohen, and S. M. LaValle, "Sensor beams, obstacles, and possible paths," in *Proc. Workshop Algorithm. Found. Robot.*, 2008, p. 14.
[44] B. Tovar and S. M. LaValle, "Visibility-based pursuit-evasion with bounded speed," *Int. J. Robot. Res.*, vol. 27, pp. 1350–1360, 2007.
[45] B. Tovar, R Murrieta, and S. M. LaValle, "Distance-optimal navigation in an unknown environment without sensing distances," *IEEE Trans. Robot.*, vol. 23, no. 3, pp. 506–518, Jun. 2007.
[46] V. Turetsky, "Upper bounds of the pursuer control based on a linear-quadratic differential game," *J. Optim. Theory Appl.*, vol. 121, no. 1, pp. 163–191, Apr. 2004.
[47] R. Vidal, O. Shakernia, H. J. Kim, D. H. Shim, and S. Sastry, "Probabalistic pursuit-evasion games: Theory, implementation, and experimental evaluation," *IEEE Trans. Robot. Autom.*, vol. 18, no. 5, pp. 662–669, Oct. 2002.
[48] C.-C. Wang, C. Thorpe, S. Thrun, M. Hebert, and H. Durrant-Whyte, "Simultaneous localization, mapping and moving object tracking," *Int. J. Robot. Res.*, vol. 26, no. 9, pp. 889–916, 2007.
[49] I. Yan and G. L. Blankenship, "Numerical methods in search path planning," in *Proc. 27th IEEE Conf. Decis. Control*, 1988, vol. 2, pp. 1563–1569.
[50] D. B. Yang, H. H. Gonzalez-Banos, and L. J. Guibas, "Counting people in crowds with a real-time network of simple image sensors," in *Proc. IEEE Int. Conf. Comput. Vision*, 2003, vol. 1, pp. 122–129.
[51] J. Yu and S. M. LaValle, "Tracking hidden agents through shadow information spaces," in *Proc. IEEE Int. Conf. Robot. Autom.*, 2008, pp. 2331–2338.
[52] J. Yu and S. M. LaValle, "Probabilistic shadow information spaces," in *Proc. IEEE Int. Conf. Robot. Autom.*, 2010, pp. 3543–3549.

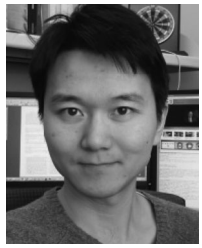

Jingjin Yu (S'11) received the B.S. degree in materials engineering from the University of Science and Technology of China, Hefei, China, in 1998, the M.S. degree in chemistry from the University of Chicago, Chicago, IL, in 2000, the M.S. degree in mathematics from the University of Illinois at Chicago in 2001, and the M.S. degree in computer science from the University of Illinois at Urbana-Champaign in 2010, where he is currently working toward the Ph.D. degree with the Department of Electrical and Computer Engineering.

His research interests include robotics and control theory.

Steven M. LaValle (M'95) received the B.S. degree in computer engineering and the M.S. and Ph.D. degrees in electrical engineering, from the University of Illinois at Urbana-Champaign, in 1990, 1993, and 1995, respectively.

From 1995 to 1997, he was a Postdoctoral Researcher and Lecturer with the Department of Computer Science, Stanford University, Stanford, CA. From 1997 to 2001, he was an Assistant Professor with the Department of Computer Science, Iowa State University, Ames. He is currently a Professor with the Department of Computer Science, University of Illinois at Urbana-Champaign. He is the author of *Planning Algorithms* (Cambridge, U.K.: Cambridge Univ. Press, 2006). His research interests include planning algorithms, sensing, motion planning, computational geometry, and control theory.